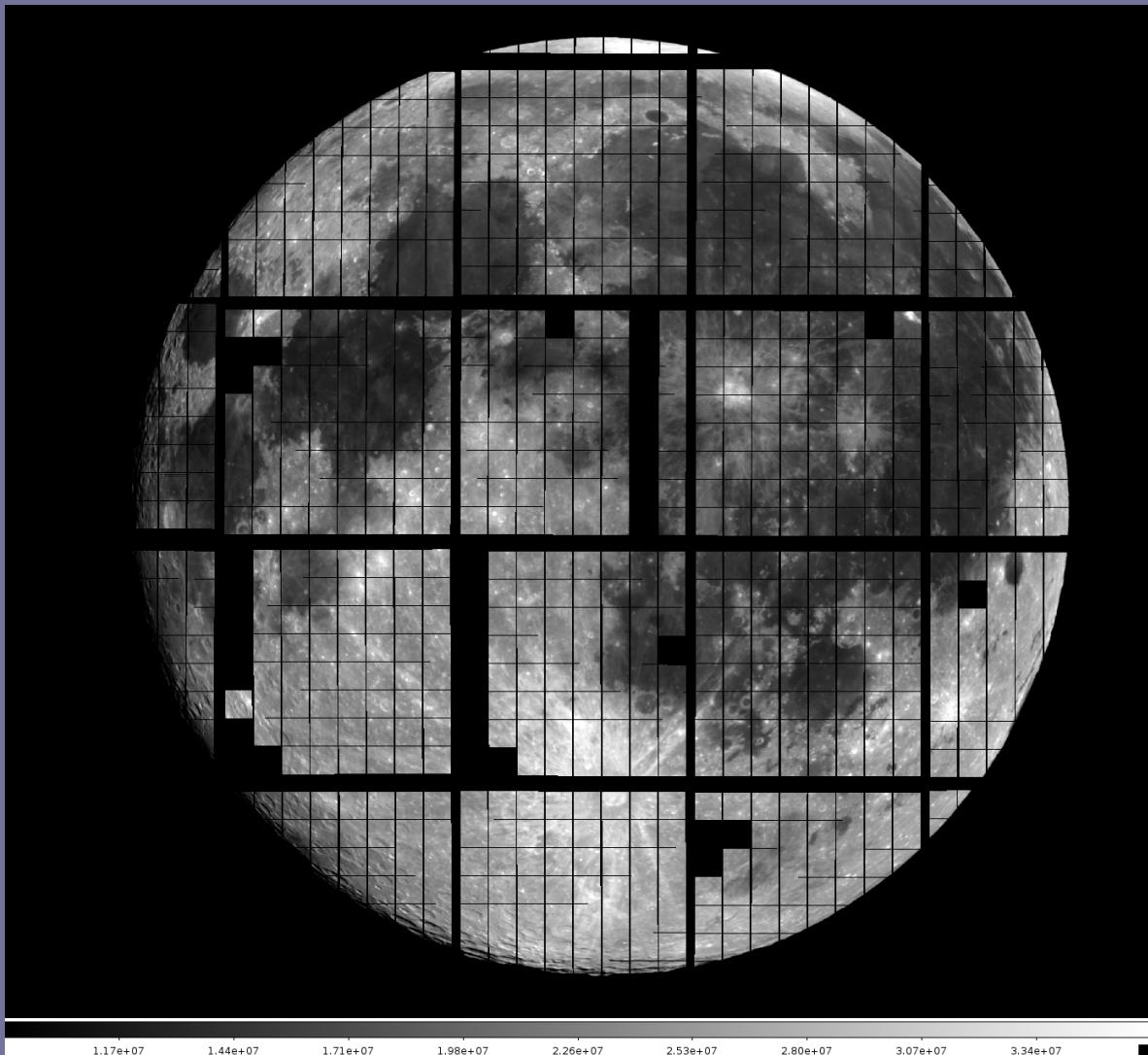


# The WIYN One Degree Imager User Manual



Version: 4.1

Generated: February 27, 2017

SVN Rev: 183

© 2012-2016 WIYN Consortium, Inc.



**Summary:**

This is the ODI Operating Manual and is a recommended read for anybody using or operating the ODI instrument.

**Signoff for Version 2:**

WIYN ODI Scientist	Daniel Harbeck	July 1 2014
--------------------	----------------	-------------

**Revision History:**

Version	Date	Author	Changes
1	5/30/2013	D. Harbeck	First public release.
2	9/11/2013	D. Harbeck	Updated GUI figures, include binning, misc.
3	6/1/2014	D. Harbeck & Wilson Liu	Update on calibration stability, guide star prediction, pointing correction. Overall update.
4	July 2015	D. Harbeck	Work in progress for 5x6 ODI.



**Notes:**

1. *no notes available at this time*

---

*Title picture:  
A 5 millisecond exposure of the moon observed by 5x6 ODI.*

# Contents

<b>1</b>	<b>Instrument Overview</b>	<b>7</b>
1.1	Instrument Walk-Through . . . . .	8
1.1.1	Instrument Body . . . . .	8
1.1.2	Major External Components & Infrastructure . . . . .	10
1.2	The ODI Focal Plane . . . . .	11
1.2.1	OTA Detectors . . . . .	11
1.2.2	pODI with 13 detectors (2012 - 2014) . . . . .	11
1.2.3	ODI with 30 detectors (2015- ...) . . . . .	12
1.2.4	Coordinate Systems in ODI . . . . .	13
1.2.5	Understanding ODI Images - A directory of FITS files . . . . .	13
<b>2</b>	<b>ODI Detector &amp; Imaging Performance</b>	<b>17</b>
2.1	Image Quality . . . . .	17
2.1.1	Sensitivity . . . . .	17
2.1.2	Read Noise, Gain, Full Well . . . . .	17
2.1.3	Amplifier and Pass Transistor Glow . . . . .	20
2.1.4	Dark Current . . . . .	20
2.1.5	Crosstalk . . . . .	21
2.1.6	Persistent Charge / Ghost Images . . . . .	21
2.1.7	Fringing . . . . .	22
2.1.8	Charge Transfer Efficiency of Lot 6 detectors . . . . .	22
2.1.9	Vignetting . . . . .	23
2.1.10	Imaging Quality . . . . .	23
2.1.11	Linearity & Photometry . . . . .	24
2.1.12	Astrometry . . . . .	26
2.1.13	Calibration Stability and Artifacts . . . . .	29
<b>3</b>	<b>Observing with ODI</b>	<b>35</b>
3.1	Understanding the data flow in guided & OT corrected images . . . . .	36
3.1.1	Open-Loop OT Correction vs. Closed-Loop Telescope Guidance . . . . .	37
3.2	Overview of ODI Tools . . . . .	38
3.3	The ODI Menu . . . . .	38
3.4	Launching Observations with the ODI GUI . . . . .	39
3.4.1	The Login Screen . . . . .	39



3.4.2	Ad hoc observations . . . . .	40
3.4.3	Standard Dome Calibrations . . . . .	45
3.4.4	Dither Patterns . . . . .	47
3.5	Manual Filter & ADC Control . . . . .	47
3.5.1	Filter Operation . . . . .	48
3.5.2	ADC Operations . . . . .	48
3.6	The ODI File Browser . . . . .	48
3.6.1	Image Actions and Image Display . . . . .	50
3.7	The OTAListener . . . . .	51
3.7.1	Overview Image . . . . .	53
3.7.2	Single OTA Display & Guide Star Selection . . . . .	53
3.7.3	Correcting the Telescope Pointing Zero Point . . . . .	53
3.8	Telescope Guider Application . . . . .	54
3.8.1	Non-sidereal tracking . . . . .	56
3.9	Where are My Data? . . . . .	57
3.9.1	Quick Reduce Data . . . . .	57
3.9.2	Obtaining help . . . . .	58
<b>4</b>	<b>ODI Observing Strategies &amp; Hints</b>	<b>59</b>
4.1	Starting to Observe: A Walkthrough . . . . .	59
4.1.1	Afternoon . . . . .	59
4.1.2	Evening . . . . .	60
4.2	Guide Star Selection . . . . .	61
4.2.1	Automatic Guide Star Selection . . . . .	61
4.3	Exposure Time Calculator . . . . .	63
4.4	Dithering . . . . .	63
4.5	Telescope Guiding & OT Corrections . . . . .	63
4.6	Filters . . . . .	64
4.7	Pointing offsets for ODI . . . . .	64
4.7.1	Correcting Telescope Pointing using ODI . . . . .	64
4.8	Observing Overheads . . . . .	66
<b>5</b>	<b>Afternoon Calibrations and the ODI Standard Calibration Plan</b>	<b>67</b>
5.1	Summary of standard calibration plan observations . . . . .	68
<b>A</b>	<b>Software Operations &amp; Known Issues</b>	<b>71</b>
A.1	Known Issues . . . . .	71
A.1.1	Stargrasp Controllers GH become unresponsive . . . . .	71
A.1.2	Readout stalls for a while, but resumes . . . . .	71
A.1.3	Readout stalls and does not finish, with error messages such as DAC busy. . . . .	72
A.2	Walkthrough: Bringing up the ODI Observing Environment . . . . .	72
A.3	Starting and Shutting Down the ODI Computer System . . . . .	74
A.3.1	Restarting the JBOSS Application Server on <code>odiweb</code> . . . . .	74
A.3.2	Restarting the JBOSS Application Server on <code>odiserv</code> . . . . .	75



A.3.3	Starting the ODI Database System (Oracle) . . . . .	75
<b>B</b>	<b>Starting Observations on the Command Line</b>	<b>77</b>
<b>C</b>	<b>When Images Look Wrong</b>	<b>79</b>
C.1	Flat Field: The Tertiary Mirror at Wrong Port . . . . .	79
C.2	Condensation on Dewar Window . . . . .	80
C.3	Vacuum Ion Gauge enabled . . . . .	80
C.4	Residual Charge in Detectors I: After Powering On . . . . .	81
C.5	Residual Charge in Detectors II: Darks . . . . .	81

# Chapter 1

## Instrument Overview

Telescope & Port	WIYN 3.5m telescope, permanently mounted at f/6.3 Nasmyth port
Field of View	pODI (2012-2014): $24' \times 24'$ ODI (2015- ... ): $40' \times 48'$
Optics	2-element field flattener & atmospheric dispersion compensator
Detectors	pODI (2012-2014): $13 \times$ STA OTA CCDs ODI (2015- ... ): $30 \times$ STA OTA CCDs full design: $64 \times$ STA OTA CCDs
Pixel Scale	$12 \mu\text{m}$ , $0.11''$ / pixel
OTA Cell Size	$480 \times 494$ pixels; $52'' \times 54''$ on sky
Gaps between cells	x: 28 pixels ( $3''$ ); y: 11 pixels ( $1.3''$ )
Gaps between OTAs	about $21''$
Fill Factor per OTA	90%
Read noise	$\leq 10 e^-$ , $8.5 e^-$ typ.
Gain	typ. $1.1 - 1.6 e^-/\text{ADU}$ , varies by cell
Dark Current	$0.006 e^-/\text{sec}/\text{pixel}$ typical
Exposure time	Minimum $\sim 5$ ms. Maximum limited by OTA amplifier glow. Linear from 20 ms to 60 min.
Filters	Full size filters: g' r' i' z' compatible w/ KPNO Mosaic filters w/ smaller FoV
Readout time	$\leq 30$ seconds sustained bias to bias
Humidity range	$\leq 70\%$

**Table 1.1:** ODI in a nutshell.

## 1.1 Instrument Walk-Through

ODI consists of the instrument body that is mounted to the Nasmyth port of the WIYN telescope plus supporting infrastructure throughout the WIYN facility. In this chapter we will discuss the major components of the instrument hardware, the properties of the detectors and how they are arranged on the focal plane, and the support infrastructure for ODI.

### 1.1.1 Instrument Body

The instrument main body is divided into three major components:

The **Forward Corrector Element** that mounts into the Nasmyth port. Its sole purpose is to position the first optical element of ODI, the forward corrector (also called Lens 1, see Fig. 1.1 (a)).

The **Instrument Support Package** (ISP) (bolted to the forward corrector element) is the backbone of the instrument and hosts the following elements (see Fig. 1.1):

1. Two rotatable prisms that constitute an atmospheric dispersion compensator. Each prism is driven by a stepper motor and has end switches.
2. Nine filter arms that move into the telescope beam like a semaphore. The filter arms are mounted to three supporting posts (labeled A, B, C). On each post there are three filter arms mounted (labeled 1, 2, 3, where 1 is the one closest to the telescope). Each filter arm has its own stepper motor and gear box.
3. The Bonn shutter.
4. Temperature sensors and a temperature multiplexer box.

The **dewar** is mounted to the ISP. Its main component is the vacuum vessel with the focal plane. The dewar window is also an optically powered element, and forms the field flattener in conjunction with the forward corrector lens. The focal plane with up to 64 OTA detectors is cooled by four closed-cycle helium cryo-heads that are capable of removing 200W of heat from the focal plane ( $\approx 120$  W for a full set of 64 OTA detectors, plus about 60W radiative load). You will also find a turbo-molecular vacuum pump permanently mounted to the dewar.

The CCD controllers (IfA Stargrasp controllers) are mounted on two opposite sides of the dewar, and each side drives one half of the detector array on the focal plane. Since the CCD controllers dissipate a significant amount of heat (1.2kW), they are enclosed in isolated, glycol-cooled boxes to avoid creating a turbulent air flow in the dome (and thus diminishing the seeing).



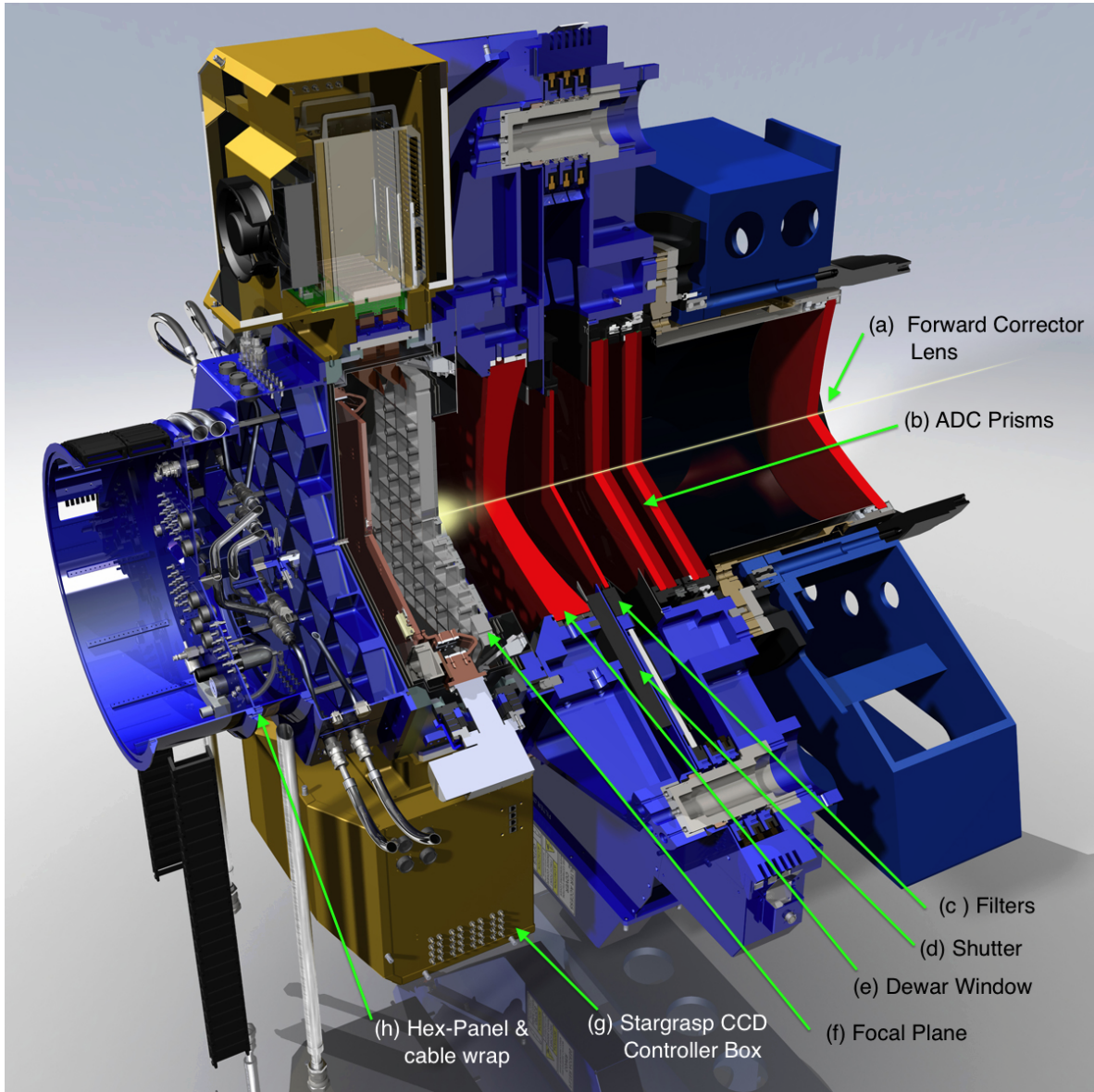


**Figure 1.1:** Cut through ODI Model. Light enters from the telescope (right) through the forward corrector lens (a), then passes the two prisms of the atmospheric dispersion compensator (b) and one of the nine filters (c). Following the filters the shutter (d) is mounted just in front of the dewar window (e); note that the dewar window also has optical power. In the dewar the detectors are mounted on the focal plane (f). Noticeably mounted on the sides of the dewar are the two golden Stargrasp CCD controller boxes (g). The hex panel and cable wrap (h) are mounted on the back of the instrument.



On the backplane of the dewar the *hex-panel* is mounted. The hex-panel is the interface for various cable, glycol, dry air, and helium connections that are routed through a cable warp to a boom hanging over the instrument.

### 1.1.2 Major External Components & Infrastructure

ODI depends on external infrastructure and components that either could not be mounted on the instrument body due to weight constraints, or for other practical considerations. These components are in particular:

1. **ISP control computer:** The ISP Control Computer is mounted to the telescope fork. It controls the helium cryo-heads, the thermal regulation and heating of the focal plane, overall instrument temperature telemetry, ADC prism and filter arm motors. The box also provides power for the shutter and monitors the shutter's state. While not critically dependent on cooling, the ISP box is glycol cooled for thermal management.
2. The **Stargrasp Power Supply Box** provides the electrical power to the Stargrasp CCD controllers. Since the power supplies also dissipate a significant amount of heat, it is also linked to the glycol cooling system. Indeed, the control node for the glycol system is located in that box. In order to keep the lines short, the main power lines are routed directly from the power supply box to the hex panel, bypassing the cable wrap.
3. Heat removal from the instrument is achieved through the **ODI Fluid Chiller & glycol heat exchanger** system. This system consists of the fluid chiller in the WIYN utility room, and a heat exchanger outside the WIYN building.
4. The **ODI helium compressors** in the WIYN utility room supply the cryo heads on the ODI dewar with pressurized helium to cool the focal plane. The waste heat from the helium compressors is dissipated in a heat exchanger unit outside the WIYN building. Helium lines are routed through the telescope pier to the instrument.
5. The **ODI data acquisition computer rack & network switches** are located in the WIYN computer cabinet. A dedicated 10-Gigabit switch routes data coming from the 32 Stargrasp fiber pairs to the ODI data acquisition computer.
6. The **ODI Observer Computer** is a Mac Pro computer with two 30 inch displays, located in the WIYN control room.

## 1.2 The ODI Focal Plane

### 1.2.1 OTA Detectors

A significant design driver for ODI — in addition to the large field of view — was to deliver and actively increase the already excellent image quality that the WIYN site is known for. In addition to passive measures (field flattener and ADC, thermal management), active tip/tilt image compensation can be deployed using *Orthogonal Transfer Array* (OTA) CCDs. This type of CCD detector allows to compensate for image motion electronically in the detector (see Fig. 1.2). While regions in a single OTA detector can be used to trace the actual image motion by monitoring bright stars, the charge in integrating cells can be shifted to follow the optical image in real-time, and thus compensate for motion blur.

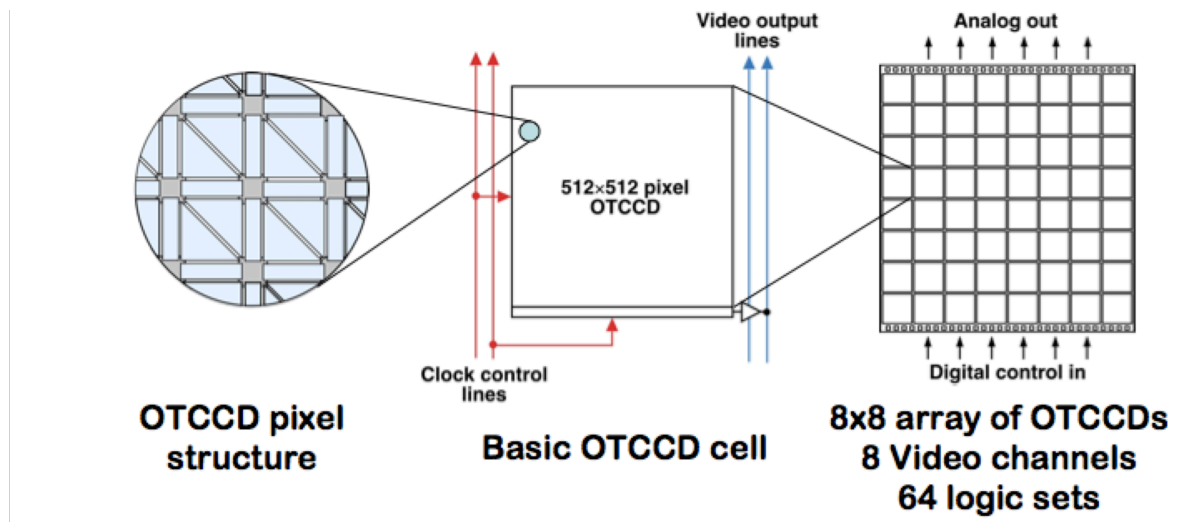


**Figure 1.2:** Concept of the Orthogonal Transfer Array (OTA) detector: The structure of the single pixels (left) allows controlled charge movement up and down (as in a conventional CCD), and to the left or right in a given cell. Thus, the charge image, as it builds up during an exposure, can be made to follow the moving optical image. Each individual OTA detector (right) is divided into an  $8 \times 8$  array of individual OT Cells (middle, ODI OTAs have actually  $480 \times 494$  pixels per cell, about  $1' \times 1'$  on sky) that share some clocking and output lines, but with some restrictions can be considered to be independent detectors. The video signal of cells with a bright star can be used to measure the actual image motion, that can then be corrected for in the other remaining OTAs.

### 1.2.2 pODI with 13 detectors (2012 - 2014)

While ODI was originally designed for an array of 64 detectors to cover the full one degree field of view, the first incarnation was only partially (hence pODI) populated with 13 detectors.

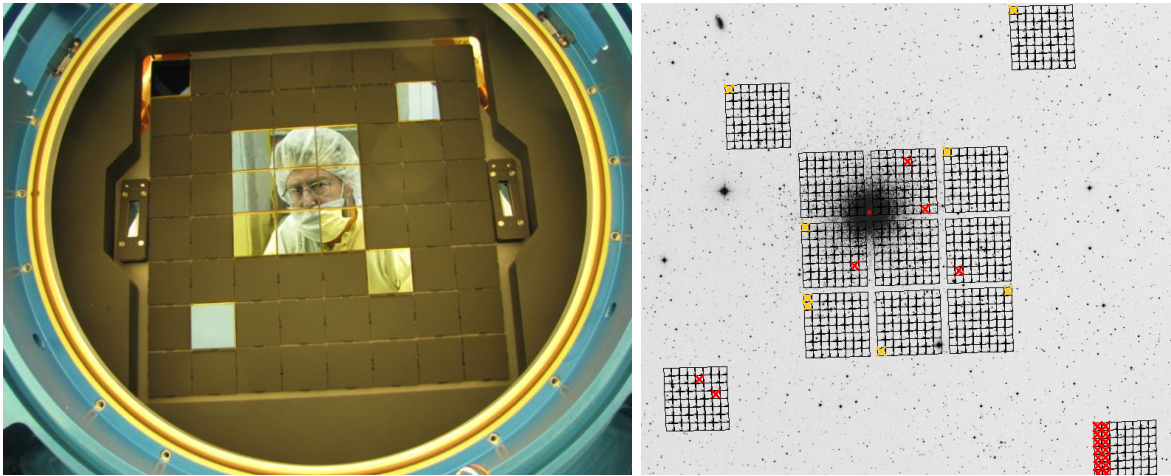


**Figure 1.3:** In pODI (2012 - 2014), 13 detectors are mounted on the focal plane (left). The imprint on the sky is shown right; in that image north is up, east is left. Note that the actual pixel coordinate system of pODI is swapped in the east/west direction. In the imprint map, defective OTA cells are marked with red crosses; cells that are unable to perform efficient OT corrections are marked with yellow crosses.

The vacant slots in the focal plane are covered with blackened aluminum blanks to reduce the possibility of reflections (see Fig. 1.3).

### 1.2.3 ODI with 30 detectors (2015- ...)

During the Winter of 2014 / 2015 17 additional devices were added to the ODI focal plane. The new devices originated mostly (16 of them) from a new OTA production Lot ("Lot 7"), where the low light level CTE problem has been resolved. The new Lot 7 detectors were arranged into a 4x4 array, with the remaining Lot 6 detectors padding the central square to a total 5x6 array of detectors, or a field of view of 40' × 48' on sky.

During production of the Lot 7 devices it was discovered that aging of the ceramic carriers caused an issue with epoxy wetting the entire carrier surface. This results in some epoxy voids in the detectors, that can be seen in images as extended structures. At the time of this writing, the epoxy underfill areas do flat-field correctly.

Whereas the new Lot 7 detectors are not impacted by the low light level problem, the remaining Lot 6 devices are, and when using the full field of view of the 5x6 configuration observations should be planned accordingly.

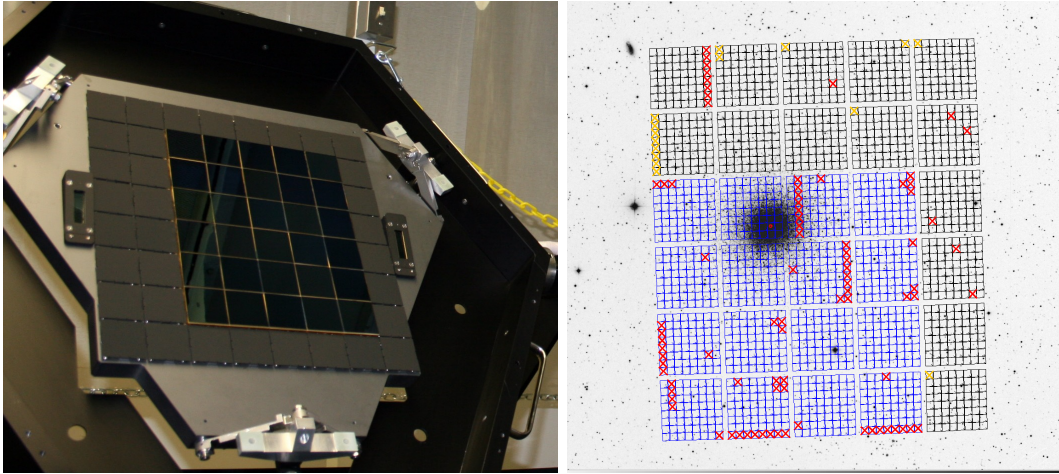


**Figure 1.4:** A total of 30 detectors ( a mixture of one Lot3, thirteen Lot 6, and 16 Lot 7 detectors) is mounted in the 5x6 ODI (2015 - ) focal plane. As in pODI, the logical pixel coordinate system is swapped with respect to the standard east-west orientation.

### 1.2.4 Coordinate Systems in ODI

A pixel in ODI can be uniquely identified by three coordinates:

1. The OTA detector, which is identified by its X/Y position on an  $8 \times 8$  grid on the focal plate, as identified in Fig. 1.5.
2. The Cell within an OTA, which is identified by its X/Y position on an  $8 \times 8$  grid on the OTA, as identified in Fig. 1.6. Note that the cell Y axis is anti-parallel to the OTA Y and pixel Y axis.
3. The pixel X/Y coordinate within an OTA cell.

Thus, a pixel can be identified by these three coordinates pairs: OTA X/Y, Cell X/ Y, and Pixel X/Y. The ODI raw FITS format, and all instrument software, work in the natural pixel coordinate system. Therefore, images at the telescope will display north up, and east right.

### 1.2.5 Understanding ODI Images - A directory of FITS files

The complexity of the focal plane and detector architecture is reflected in the raw ODI images. The image size of  $\geq 2$ GB for a full ODI image puts further constraints on a usable file format, forcing to split a full readout into several files. As a consequence, each ODI image readout is stored in an individual directory. Within each directory there are a large number of files, but at the core there are \*\_XY.fits files that contain the actual image. There is one MEF FITS

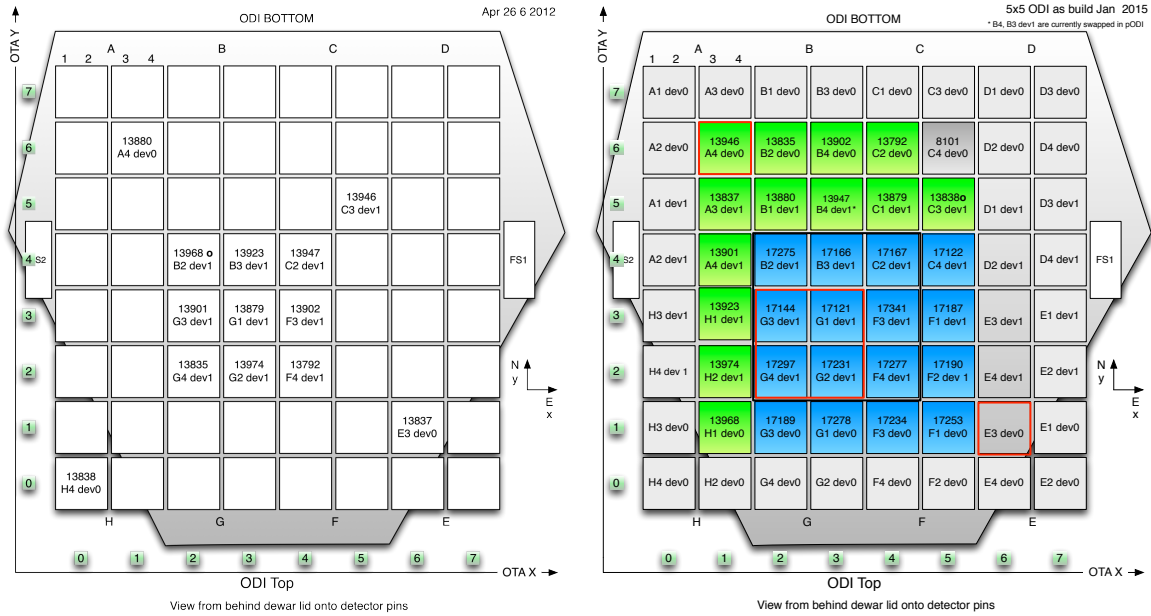


**Figure 1.5:** Left: pODI focal plane layout. There are 13 OTA detectors populated out of the 64 possible locations. Right: 5x6 ODI focal plane layout. To the left and right, two focus sensors are mounted. For each of the OTA detectors, the device’s serial number and the Stargrasp controller address are given. The Stargrasp controller address consists of a letter (A through H, identifying a chassis of four controller boards), the board number in that chassis, and one of the two devices that a board can drive. Individual detectors are shortly identified by their X and Y coordinate on the focal plane (numbers with green background).

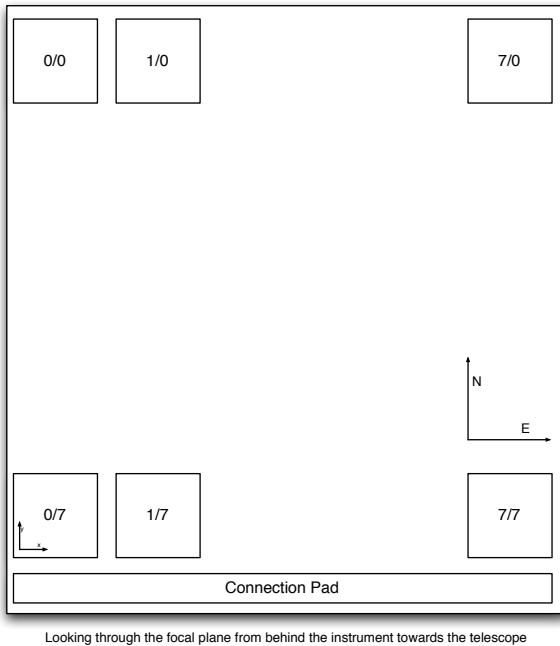


**Figure 1.6:** Coordinate system in a single back-side illuminated OTA device. Pixel coordinates increment from the lower left to the upper right. Cells are identified by numbers from 0 to 7. Cell-X coordinates increment from left to right, cell-Y coordinates increment from the top to the bottom, i.e., opposite to the pixel coordinates in the y direction.

Console	Date Modified	Size	Kind
exposure.log	Today 3:08 AM	2.3 MB	Log File
Show items as icons, in a list, in columns, or with Cover Flow			
preimage	Today 3:02 AM	--	Folder
expVideo	Today 3:03 AM	--	Folder
temp	Today 3:08 AM	--	Folder
Preview			
o20121120T030221.0.23.bin8.jpeg	Today 3:08 AM	177 KB	JPEG image
o20121120T030221.0.24.bin8.jpeg	Today 3:08 AM	149 KB	JPEG image
o20121120T030221.0.23.bin64.jpeg	Today 3:08 AM	4 KB	JPEG image
o20121120T030221.0.24.bin64.jpeg	Today 3:08 AM	4 KB	JPEG image
o20121120T030221.0.61.bin8.jpeg	Today 3:08 AM	86 KB	JPEG image
o20121120T030221.0.55.bin8.jpeg	Today 3:08 AM	254 KB	JPEG image
o20121120T030221.0.61.bin64.jpeg	Today 3:08 AM	4 KB	JPEG image
o20121120T030221.0.32.bin8.jpeg	Today 3:08 AM	200 KB	JPEG image
o20121120T030221.0.34.bin8.jpeg	Today 3:08 AM	133 KB	JPEG image
o20121120T030221.0.44.bin8.jpeg	Today 3:08 AM	142 KB	JPEG image
o20121120T030221.0.55.bin64.jpeg	Today 3:08 AM	4 KB	JPEG image
o20121120T030221.0.32.bin64.jpeg	Today 3:08 AM	4 KB	JPEG image
o20121120T030221.0.34.bin64.jpeg	Today 3:08 AM	3 KB	JPEG image
o20121120T030221.0.44.bin64.jpeg	Today 3:08 AM	3 KB	JPEG image
o20121120T030221.0.33.bin8.jpeg	Today 3:08 AM	182 KB	JPEG image
o20121120T030221.0.33.bin64.jpeg	Today 3:08 AM	4 KB	JPEG image
o20121120T030221.0.22.bin8.jpeg	Today 3:08 AM	185 KB	JPEG image
o20121120T030221.0.22.bin64.jpeg	Today 3:08 AM	4 KB	JPEG image
o20121120T030221.0.00.bin8.jpeg	Today 3:08 AM	84 KB	JPEG image
o20121120T030221.0.16.bin8.jpeg	Today 3:08 AM	101 KB	JPEG image
o20121120T030221.0.00.bin64.jpeg	Today 3:08 AM	3 KB	JPEG image
o20121120T030221.0.16.bin64.jpeg	Today 3:08 AM	3 KB	JPEG image
o20121120T030221.0.42.bin8.jpeg	Today 3:08 AM	175 KB	JPEG image
o20121120T030221.0.42.bin64.jpeg	Today 3:08 AM	4 KB	JPEG image
o20121120T030221.0.43.bin8.jpeg	Today 3:08 AM	152 KB	JPEG image
o20121120T030221.0.43.bin64.jpeg	Today 3:08 AM	3 KB	JPEG image
o20121120T030221.0.jpeg	Today 3:08 AM	3.5 MB	JPEG image
SAOImage D59			
o20121120T030221.0.43.fits	Today 3:08 AM	37.1 MB	Flexi...stem
o20121120T030221.0.16.fits	Today 3:08 AM	37.1 MB	Flexi...stem
o20121120T030221.0.24.fits	Today 3:08 AM	37.1 MB	Flexi...stem
o20121120T030221.0.32.fits	Today 3:08 AM	37.1 MB	Flexi...stem
o20121120T030221.0.44.fits	Today 3:08 AM	37.1 MB	Flexi...stem
o20121120T030221.0.42.fits	Today 3:08 AM	37.1 MB	Flexi...stem
o20121120T030221.0.22.fits	Today 3:08 AM	37.1 MB	Flexi...stem
o20121120T030221.0.23.fits	Today 3:08 AM	37.1 MB	Flexi...stem
o20121120T030221.0.55.fits	Today 3:08 AM	37.1 MB	Flexi...stem
o20121120T030221.0.00.fits	Today 3:08 AM	37.1 MB	Flexi...stem
o20121120T030221.0.34.fits	Today 3:08 AM	37.1 MB	Flexi...stem
o20121120T030221.0.61.fits	Today 3:08 AM	37.1 MB	Flexi...stem
o20121120T030221.0.33.fits	Today 3:08 AM	37.1 MB	Flexi...stem
TextEdit			
o20121120T030221.0.43.txt	Today 3:08 AM	349 KB	Plain Text
o20121120T030221.0.24.txt	Today 3:08 AM	350 KB	Plain Text
o20121120T030221.0.16.txt	Today 3:08 AM	349 KB	Plain Text
o20121120T030221.0.42.txt	Today 3:08 AM	349 KB	Plain Text
o20121120T030221.0.23.txt	Today 3:08 AM	349 KB	Plain Text
o20121120T030221.0.44.txt	Today 3:08 AM	349 KB	Plain Text
o20121120T030221.0.00.txt	Today 3:08 AM	349 KB	Plain Text
o20121120T030221.0.32.txt	Today 3:08 AM	349 KB	Plain Text
o20121120T030221.0.22.txt	Today 3:08 AM	349 KB	Plain Text
o20121120T030221.0.61.txt	Today 3:08 AM	349 KB	Plain Text
o20121120T030221.0.34.txt	Today 3:08 AM	349 KB	Plain Text
o20121120T030221.0.33.txt	Today 3:08 AM	349 KB	Plain Text
o20121120T030221.0.55.txt	Today 3:08 AM	349 KB	Plain Text
Xcode			
metainf.xml	Today 3:11 AM	4 KB	XML...ument

**Figure 1.7:** Content of the *raw* image directory for exposure o20121120T030221.0: For each of the 13 detectors there is one FITS file, a factor-8 and factor-16 binned jpeg preview image each, and a .txt file containing a dump of the fits header. The *metainf.xml* file contains a directory manifest, post-observation user comments, and additional telemetry data.



file present per detector that has been read out; in the case of pODI there are consequently up to 13 FITS files. The extension XY denotes the location of an OTA detector on the focal plane.

The image of each cell within a given detector is stored as an individual FITS extension, i.e., each single MEF FITS file has 64 extensions, one per cell.

Auxiliary data are available in the image directory: jpeg images that have been down-sampled by factors of 8 or 64, extracts of the fits headers in `.txt` files, and a `metainf.xml` manifest file that contains a list of all the FITS files with checksums, additional instrument telemetry data, and user annotations for an exposure.

Images with guide star readouts can contain additional directories:

1. `preimage`

This directory contains an entire image readout containing the preimage that was used to select a guide star.

2. `expVideo`

This directory will contain the guide star video stored in FITS format, and centroid / photometry data stored in a FITS table.

3. `temp`

This directory contains auxiliary files supporting the data acquisition and debug logfiles.

Details on the image format can be found in the ODI-PPA-ICD-0001.



## Chapter 2

# ODI Detector & Imaging Performance

### 2.1 Image Quality

#### 2.1.1 Sensitivity

ODI at WIYN's sensitivity is predicted based on modeling all optically relevant components. The throughput model includes: the atmospheric extinction and telluric absorption lines, the three telescope mirrors, absorption losses in the ODI optics (two lenses and two ADC prisms), anti-reflection coating performance, and the quantum efficiency of the OTA detectors. The predicted throughput has been verified on sky in the g', r', i', and z' bands within reasonable error margins, and the differences we found are included in the throughput model as a fudge factor. The resulting as-build throughput of ODI is shown in Fig. 2.1.

The blue cut-off in ODI's sensitivity is governed by special glass (O'Hara PBL6Y) in the ADC prisms. The fall-off in the red is driven by the vanishing quantum efficiency of the ODI detectors. The peak throughput of order of 55% is the sum of all losses in the system; however, the most significant peak throughput limit is defined by the losses in the three WIYN mirrors.

#### 2.1.2 Read Noise, Gain, Full Well

Each of the 64 cells on a single OTA detector has an individual output amplifier, and depending on the location on the device, voltage supply lines differ in length, resulting in some voltage drops. Hence, the variation of the gain of the individual OTAs is significant. Typical gains for OTA detectors range from 1.2 to 1.6  $e^-$ /ADU. The read noise is typically below  $10e^-$ , and can be as low as  $\leq 6e^-$ . The distribution of read noise is shown in Fig. 2.2.

The gain of detectors varies with temperature; while this is usually not a problem for temperature-regulated detectors, the ODI detectors dissipate a significant amount of power (2W per detec-



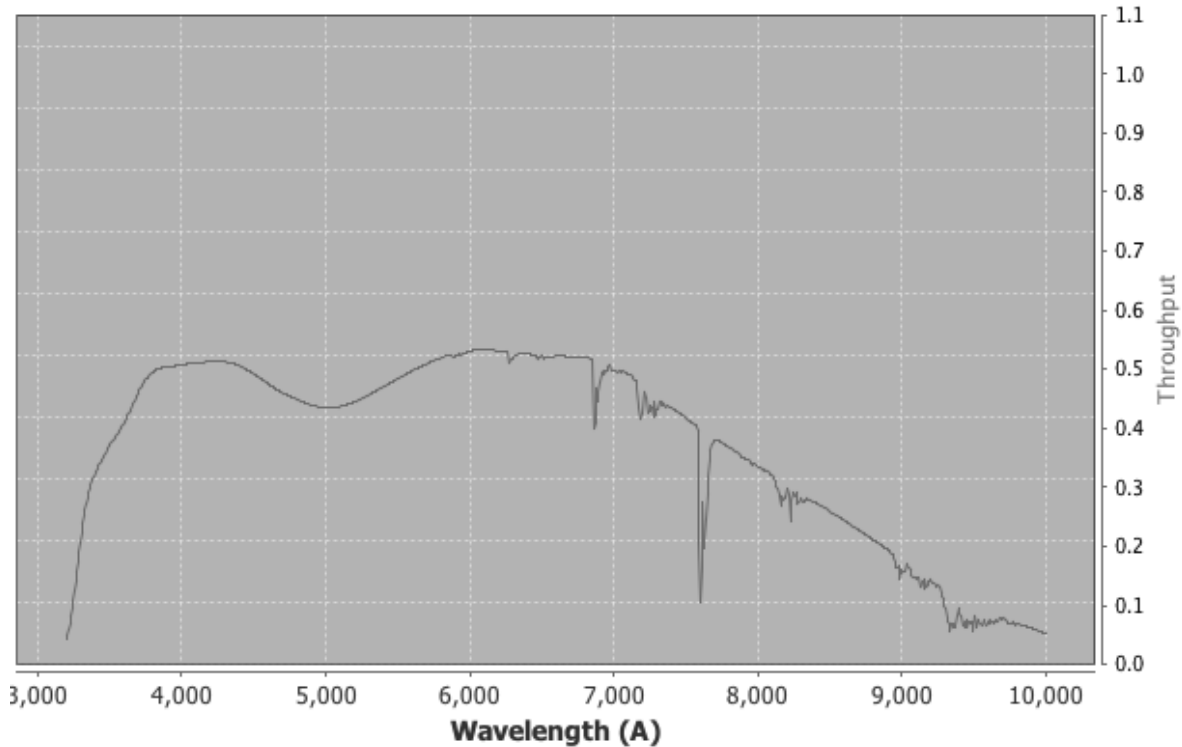


**Figure 2.1:** WIYN telescope and ODI throughput at an airmass of one. The throughput curve is based on modeling the throughput, reflectivity, and quantum efficiency of the optics and detectors, and an atmospheric extinction model. The model has then been adjusted to match actually measured zero points in the ODI filters.

tor), and hence their temperature will oscillate for one hour after powering on detectors. **In order to guarantee gain stability of ODI, there must be an hour wait time between powering on detectors and scientific (including calibration) data acquisition.**

### Gain, noise when binning

Binning with ODI has been tested and is ready to be used. However, as this mode is new and not yet fully characterized, it should be considered as shared risk operations.

With binning turned on, the ODI detector array will be read out in a  $1 \times 2$  binned mode. Physical binning at this time is applied only in the parallel clocking direction; physical binning in the serial register direction is not offered at this time due to increased read noise. However, for convenience, serial binning will be simulated by averaging in the serial readout direction, and data are stored *2 times2* binned.

Averaging data in the serial direction impacts the read noise and gain of the logical pixel, since each logical pixel contains two physical read pixels: The read noise will increase by  $\sqrt{2}$ , and

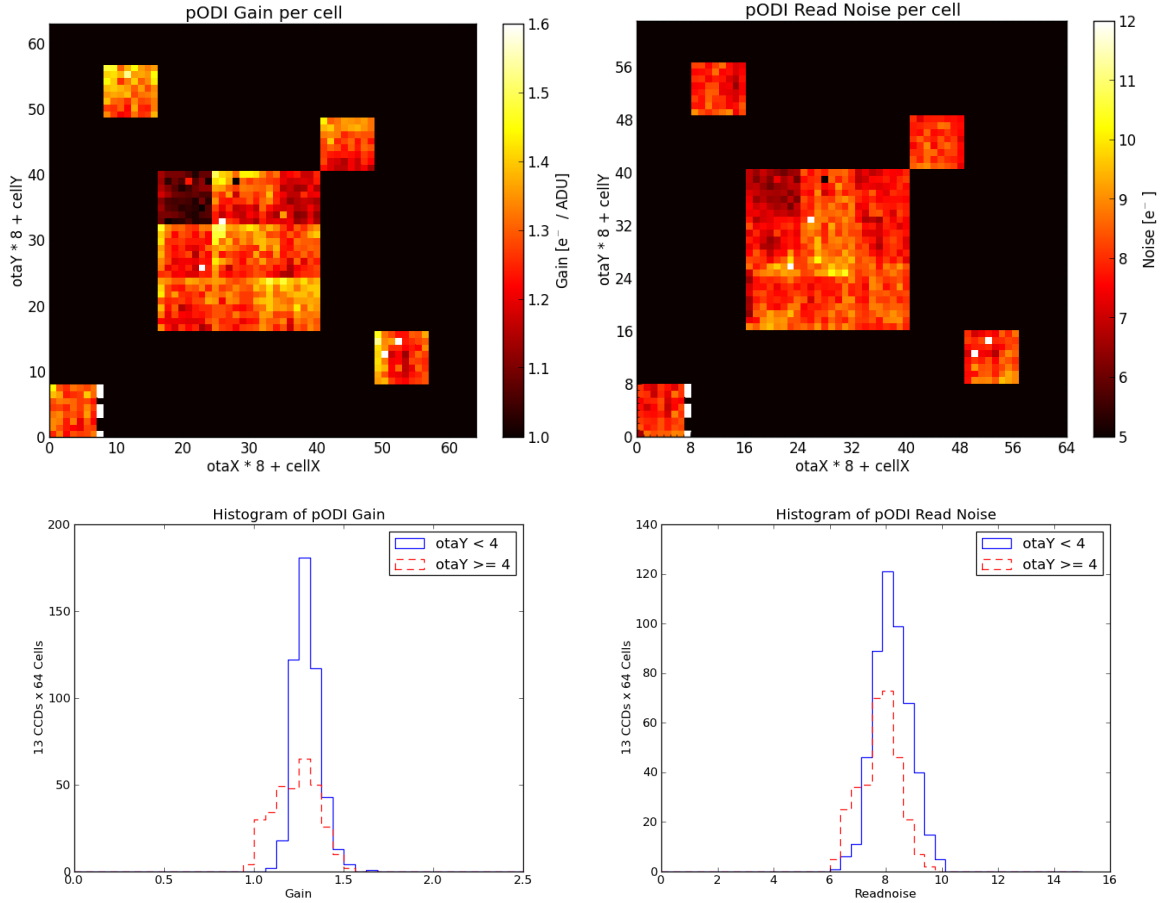


**Figure 2.2:** Top: Heat-map representation of the gain and noise for each individual cell in the pODI focal plane. Note the typical increase in the gain to the upper left of an individual OTA. The OTA at the upper left of the central array has a different doping of the amplifiers, hence the difference in gain and noise.

Bottom: Histogram of read noise and gain in the pODI focal plane. The upper and lower halves of the detectors are served by separate controller chassis; however, no significant difference in performance is apparent.

the effective gain will increase by a factor of 2 (each pixel averages two readouts). The signal to noise ratio in the read noise limited case will hence increase by  $\frac{2}{\sqrt{2}} = \sqrt{2}$ .

The benefit of binning is hence the decrease of time needed to the sky noise limit by a factor of  $\sqrt{2}$ . A second potential benefit under investigation is that the critical background level to overcome the low light level CTE problem could be achieved twice as fast.

### 2.1.3 Amplifier and Pass Transistor Glow

Transistor glow in ODI's OTA detectors remains the major limitation. The most significant source of glow are the transistors in the output amplifiers of each cell. Their glow is prohibitively high, and would dominate every exposure with exposures times above one minute. A work-around to control the amplifier glow is to reduce the drain voltage of the output amplifiers from typically 24V to 10V during any idle times, and power the amplifiers on only while detectors are read out. Therefore, output amplifier glow is reduced to a bias effect; an example bias is shown in Fig 2.3, left.

In order to facilitate the switch between science integration and active video / OT shifting mode, the parallel clocks for each cell can be driven by either a standby parallel voltage, or actively clocked parallel signals. The multiplexing between these two parallel voltages is handled by pass-transistors, and these also glow, albeit at a lower level than the transistors in the output amplifiers. Yet, in a long exposure, they start to dominate as can be seen in Fig. 2.3, right.

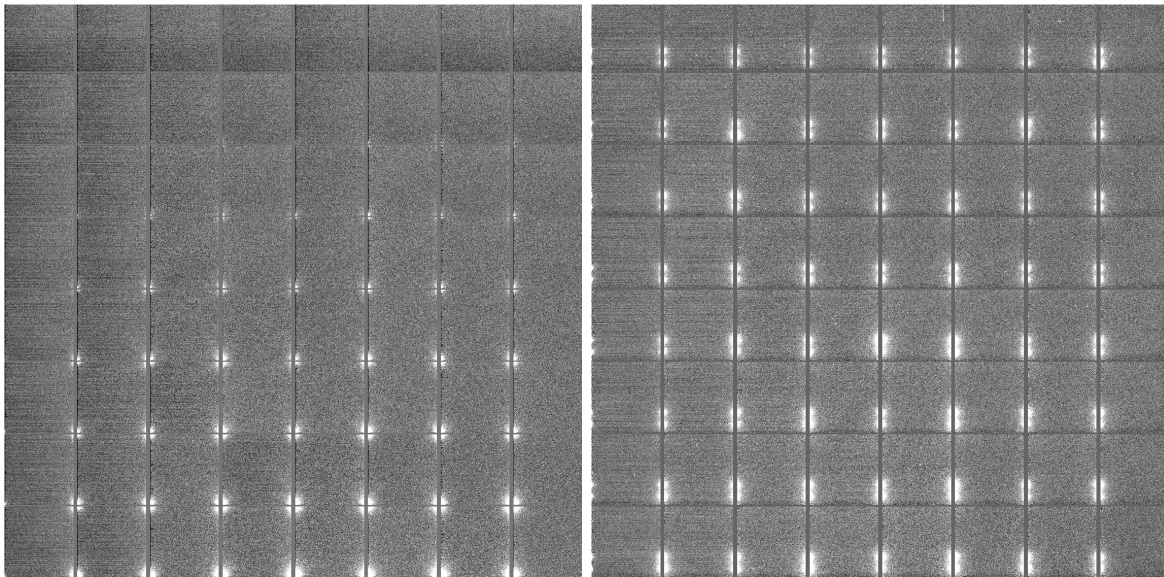


**Figure 2.3:** Example of transistor glow in a new implant level Lot 6 OTA device. Output amplifier glow in a bias (left), and pass-transistor glow in a 900 seconds dark (right).

### 2.1.4 Dark Current

A long dark exposure will have two components: The classical dark current which is generating charge in all pixels, and localized accumulating low-level amplifier and pass-transistor glow. In this section we describe the classic dark current.

Fig. 2.4 shows the distribution of dark current in the focal plane. The dark current distribution has a mean of  $0.006 \text{ e}^-/\text{pix}/\text{sec}$ , with a variance of  $0.002 (\text{e}^-/\text{pix}/\text{sec})^2$ . There is an apparent substructure in the dark current, especially with a single OTA detector, which resembles the physical structure of the OTA ceramic packages.

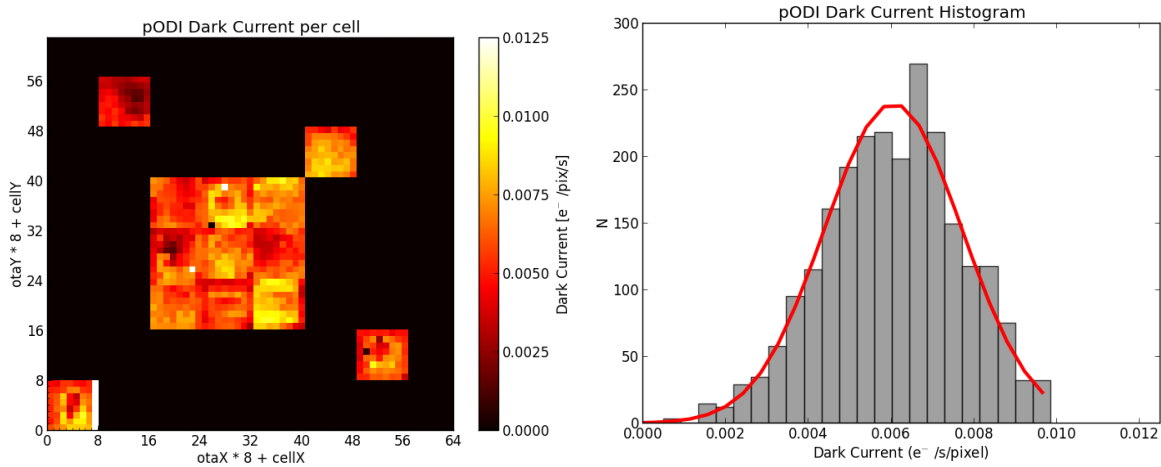


**Figure 2.4:** Dark current plotted for each OTA cell in the pODI focal plane (left), and the distribution (right).

### 2.1.5 Crosstalk

Crosstalk between output amplifiers within one OTA is present with coefficients  $\approx 5.6 \times 10^{-5}$ . It is assumed that this crosstalk is produced within a device (i.e., not controller related). Note that crosstalk will appear only between cells that are read out simultaneously, i.e., for a regular image readout, crosstalk will appear between cells in the same row (see Fig. 2.5).

Currently, there is no indication of crosstalk between different detectors.

### 2.1.6 Persistent Charge / Ghost Images

The pODI detectors are prone to retain charge and produce ghost images after significant saturation. Saturated stars will leave behind a trail in the positive y-direction, as not all charge is efficiently transported beyond the full well level. Excessive charge will also fill traps along the readout track, i.e., vertically down from a saturated star's position.

Once a trap in the imaging area is filled, it will take a prolonged time to completely clear them out. Fig. 2.6 shows a sequence of eleven subsequent readouts of the same region on a detector after observing a saturated star. The first few readouts show a strong, but declining ghost image signature, but then charge is cleared out only slowly.

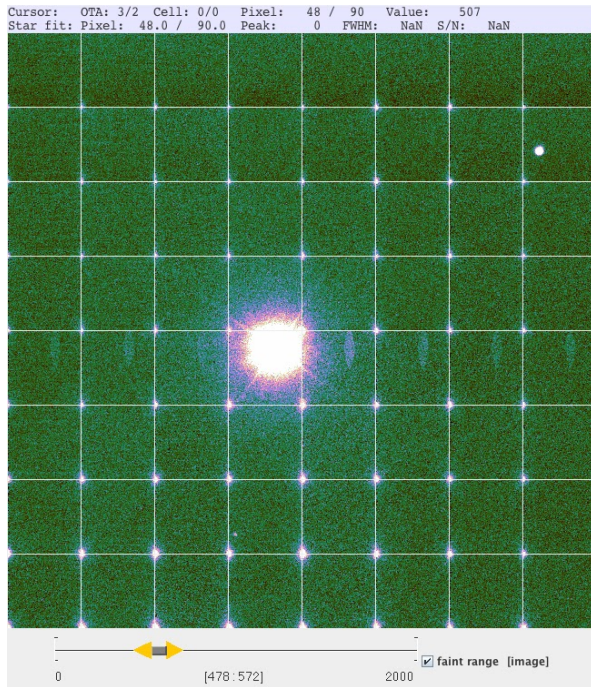


**Figure 2.5:** Cross-talk is limited within one detector to cells in the same *cell row*.

Before and after each image readout, the detectors are cleaned about five times to remove trapped charge.



Due to the slow charge release after the initial cleaning, strongly saturated stars will create ghost images in at least one or two subsequent exposures. Due to the vertical structure in the ghost image, a target of interest should not be located directly below (south) of a bright star in the same OTA cell.

### 2.1.7 Fringing

Fringing (an interference pattern caused by sky emission lines) is present at approximately a 4% level in the SDSS *z'* band, and is still present in the SDSS *i'* band. The fringe pattern has been shown to be stable on a multiple month timescale.

### 2.1.8 Charge Transfer Efficiency of Lot 6 detectors

For Lot 6 detectors (those used in pODI, and now part of the 5x6 ODI focal plane), at low light levels below about  $100e^-$ , the transfer from the imaging area into the serial register is suffering from a low charge transfer efficiency, causing trailing of stars. This phenomenon is known as "fat zero". **It is critical to expose images long enough to reach a sky level of at least  $100 e^-$ , better  $200 e^-$** , to ensure that images are not affected by the Lot 6



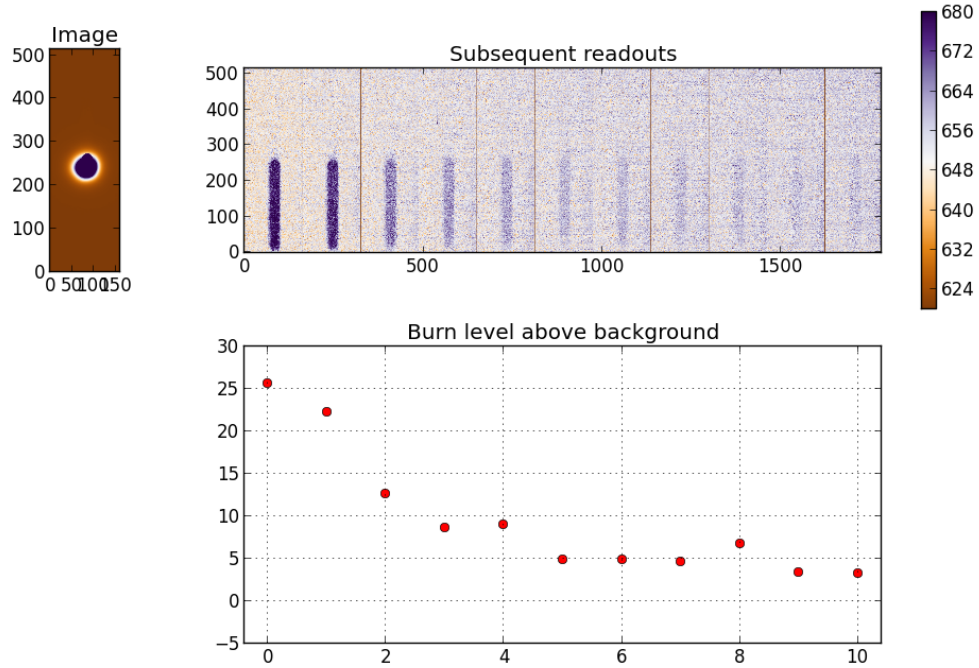


**Figure 2.6:** Persistent ghost images of saturated objects.

fat zero issue. Note that in order to be sky noise limited (instead of read noise limited), one wants to expose long enough to reach a sky level of  $\gg 10^2 = 100 e^-$  anyway, so this might be a noticeable concern only for narrow band filters.

In OTA 1/1 some cells in the lower left of the detector have a deficiency in serial charge transfer efficiency. Its behavior and impact on science are under investigation.

These restrictions do not apply to the new Lot 7 detectors in the focal plane.

### 2.1.9 Vignetting

In the pODI focal plane, only the detector in the lower left corner is affected by vignetting. The effect of vignetting is demonstrated by out of focus images of stars, which show the visible pupil on each detector.

### 2.1.10 Imaging Quality

TBD. Images in the r' band with 0.4" seeing have been recorded.

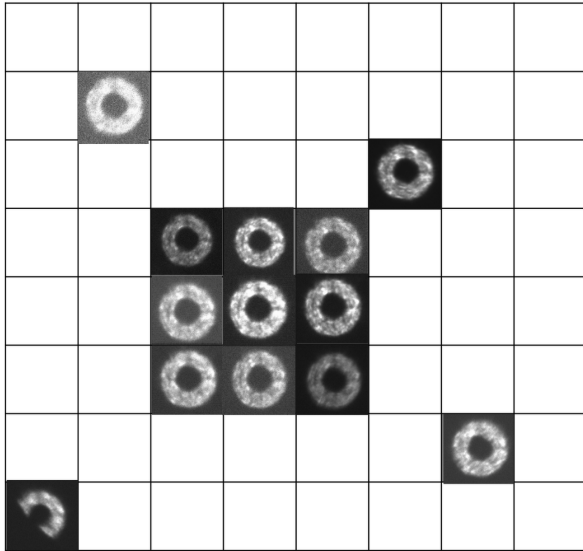


**Figure 2.7:** Vignetting across the pODI focal plane as indicated by donut (equivalent to the pupil) images. Only the OTA 0/0 is significantly affected by vignetting.

## Atmospheric Dispersion Compensator

ODI's Atmospheric Dispersion Compensator (ADC) is designed to operate in an airmass range from 1 to 2. In the  $g'$  band, using the ADC at an airmass larger than 1.2 can improve the image quality.

As the ADC prisms rotate to adjust for a range of airmass and dispersion direction, we expect an about 1% effect on the flat field. Details are subject to further study.

### 2.1.11 Linearity & Photometry

See Fig. 2.8

#### Linearity

Linearity of ODI photometry has been assessed during commissioning to be good, however, during operations in 2013 a non-linearity of the order of 2-3% has been identified. Early assessment of the non-linearity indicates that it is very well correctable with a third order polynomial function. As of this writing, routine corrections are tested in the ODI pipeline system.



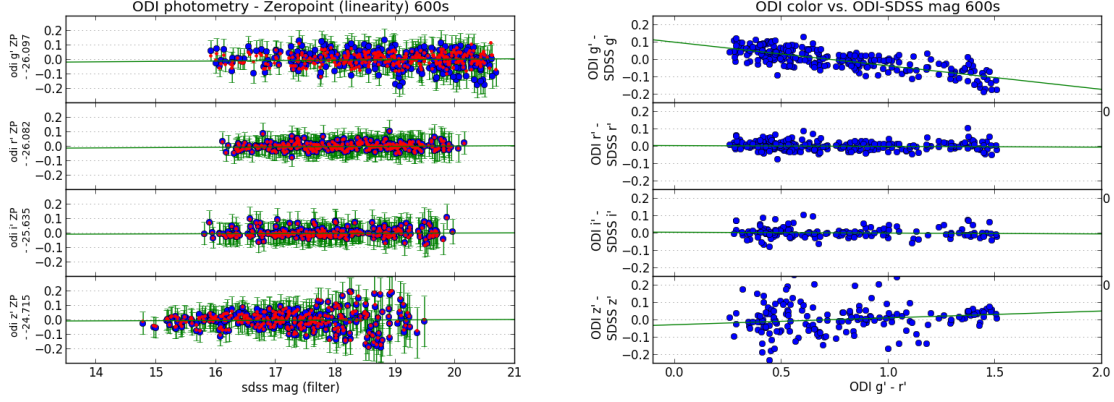


**Figure 2.8:** Left: Plot of SDSS Stripe 82 magnitudes vs. zero-point corrected ODI aperture photometry in the same filter, based on a 600 second exposure at position 22h, 0°. Blue dots represent raw photometry, red dots show photometry after color correction. Right: Instrument color plotted vs. photometric instrumental minus SDSS magnitude. The green line is a linear fit to the color-magnitude relation.

$x$	$y$	$B_1$
$(g' - r')_{ODI}$	$(g'_{ODI} - g'_{SDSS})$	-0.136
$(g' - r')_{ODI}$	$(r'_{ODI} - r'_{SDSS})$	-0.005
$(g' - r')_{ODI}$	$(i'_{ODI} - i'_{SDSS})$	-0.005
$(g' - r')_{ODI}$	$(z'_{ODI} - z'_{SDSS})$	-0.039

**Table 2.1:** Preliminary color terms for ODI Lot 6 detectors.

## Photometric Zeropoints

### Color Terms

We quantify the color correction for the four large ODI filters by comparing the ODI instrumental magnitude offset from the corresponding SDSS magnitude, depending on the ODI instrumental  $g'-r'$  color. We choose this approach to compare the ODI photometric system to the PanSTARRS system, see [Tonry et al. \(2012\)](#). In a similar way we fit

$$y = B_0 + B_1 \times x$$

, where  $x$  is the ODI instrumental  $(g' - r')_{ODI}$  color, and  $y$  is the magnitude offset in given filter, e.g.,  $(g'_{ODI} - g'_{SDSS})$ . The zero points of this relation is irrelevant, and thus we list the slope of that relation in Table 2.1:



## Faint star photometry and low background conditions

The impact of the charge transfer efficiency issue has not yet been fully explored.

### 2.1.12 Astrometry

The typical astrometric accuracy is about 6 milli arcseconds for well-exposed objects per epoch. Due to the fat zero issue, there is a strong dependence of the y-coordinate on a star's luminosity, which is discussed below.

#### The Magnitude Equation

*This section was provided by Terry Girard and Dana Casetti, Yale University*

The astrometric "magnitude equation" is seen in the pODI data explored to date, i.e., there are shifts in the centers of stellar images that are correlated with the effective magnitude of those images. The effect is quite evident along the y (declination) axis, but is not observed along the x axis thus far.

The magnitude equation results from the combination of asymmetrical image profiles and a nonlinear detector. In CCDs, it is generally attributed to less-than-ideal CTE (Charge Transfer Efficiency).

To explore the effect, several sets of pODI data have been pre-processed then run through Sextractor and the Yale 2-D Gaussian centering routine. These consist of a small number of un-dithered, short exposures [griz] taken Aug 2012 in SDSS Stripe82; dithered 30 to 60-sec exposures [rz] in Stripe82 taken Nov 2012; and dithered long (300-s) exposures [rz] within SA94 taken Oct 2012. Two methods are used to investigate the pODI mag. eq., comparison to an external astrometric catalog and internal comparison of pODI frames with different exposure times.

We use the SDSS-DR7 catalog as an external astrometric reference, in both Stripe82 and the SA94 field. Each OTA (00,16,22,23,...,55,61) is treated as a separate "unit" and transformed into a tangential projection of SDSS (RA,Dec) using second-order polynomial field terms. (Occasionally a cubic term was significant, but this was rarely so.) Residuals along x and y (RA and Dec) were then plotted versus instrumental magnitude to look for trends.

Figure 2.9 shows the y (Dec) residuals for a 30-sec g-band exposure taken in August. Data from five of the OTAs is shown, although the remaining ones show the same behavior. Simple linear fits to the five sets are made; the fitted slopes range from -9 to -21 mas/mag. Similar y-residual trends are seen in the other passbands from the August observations, and to a lesser extent in the later data sets. In all cases, slopes along x (RA) are not significant and are therefore not shown.

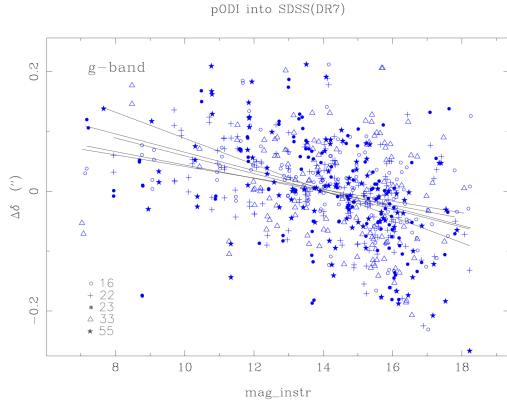


**Figure 2.9:** Residuals in  $y$  (Dec) versus instrumental magnitude following a transformation of pODI centers into SDSS(DR7) positions. Data are from a 30-sec  $g$ -band exposure in SDSS Stripe82 taken August 2012. Each OTA is handled separately. Least-squares fits to the five OTAs shown are also plotted. The slopes are on the order of 15 mas/mag and are presumed to be due to the pODI positions being affected by CTE. There are no significant trends in  $x$  (RA) residual with magnitude, which is not shown.

It is also noted that a real, cosmic relation between magnitude and proper motion, accumulated over the handful of years between the SDSS and pODI observations, could conceivably produce a trend with magnitude. A test simulation using the Besancon Galactic model indicates that over the observed magnitude range the expected effect is less than one tenth what we observe in our residual plots.

One aspect of CTE is that its effects are largest when background levels are low, (traps aren't filled in, other than by the stellar images themselves). To test this, we have fit the residual trends for all OTAs in all passbands and across all three observation sets. The fitted slopes, of both the  $y$ -residuals (upper panel) and  $x$ -residuals (lower panel) are shown in Figure 2.10. The data to the left consist of 15 to 60-sec exposures in  $g$ ,  $r$ , and  $z$ -band. The grouping to the right is of 300-sec  $r$ -band exposures in SA94. The upper panel shows the expected behavior - the linear magnitude equation in  $y$  has the largest amplitude when the background levels are low.

Note that a linear mag. eq. (astrometric shift proportional to instrumental magnitude) will not be detectable in an internal comparison of long and short exposures but higher-order magnitude terms can be seen. This is because the long-to-short astrometric solution essentially measures the differential of the magnitude equation (delta shift induced by a delta-magnitude) and, thus, a linear magnitude equation will produce a constant shift between short and long exposures, one that gets absorbed by the necessary constant term in the transformation model. On the other hand, the superior precision of the pODI internal comparison makes it possible to detect higher-order terms. 2.11 shows  $y$  residuals as a function of instrumental magnitude from a 60-sec  $r$ -band exposure transformed into a 30-sec exposure. Five of the OTAs are shown, but the others are similar. The curvature brighter than  $\text{mag}_{\text{instr}} 11$  or 12 is probably an effect of saturation. More disturbing is the significant linear trend seen in what should be the well-measured magnitude range. The slope in this figure indicates that a quadratic magnitude equation is afflicting the pODI astrometry, at least for these 30 to 60-sec exposures. The observed slope, roughly 0.15 pix/mag, corresponds to a quadratic magnitude-equation term of  $\sim 0.6 \text{ mas/mag}^2$ . This is just below the level that might be detected in Figure 2.8, because

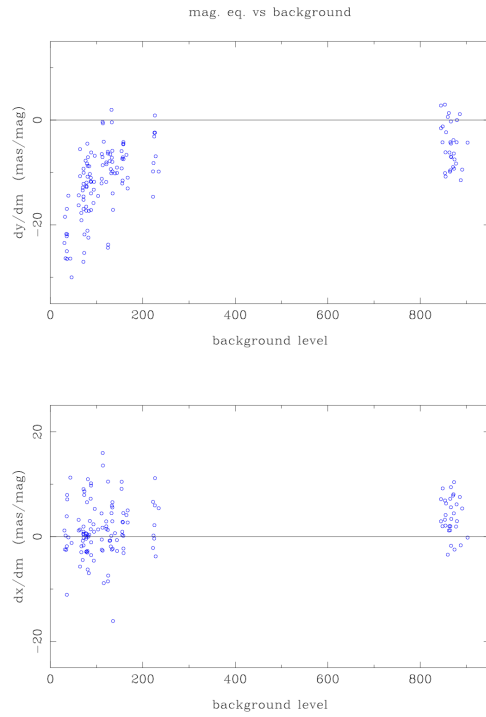


**Figure 2.10:** Slopes of y-residual (upper) and x-residual (lower) magnitude equation as a function of pODI background level. Each symbol represents an OTA that has been transformed into the SDSS reference positions. The data include observations from the three data sets, with various filters, and with various exposure times.

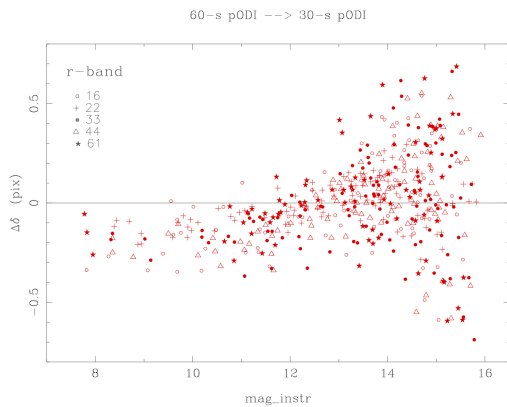


**Figure 2.11:** Residuals in y of a 60-sec pODI exposure transformed into a 30-sec exposure for a field in SDSS Stripe82. These r-band data were taken in November 2012. As before, each OTA is treated separately and the residuals stacked afterward. The linear trend over the well-measured region ( $instr. mag. = 11$  to  $15$ ) corresponds to an intrinsic magnitude equation that is (at least) quadratic in form.

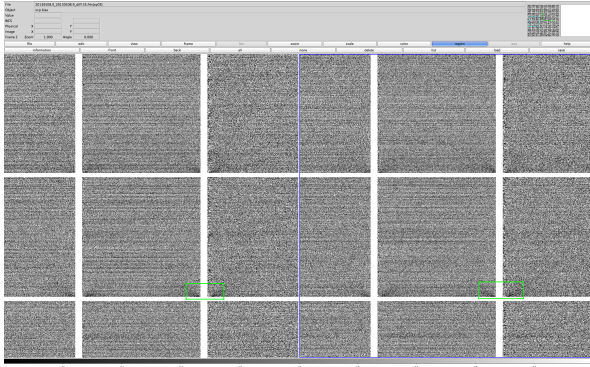


**Figure 2.12:** Difference between the first and second frames in a sequence of biases (left; time baseline  $\approx 20$ s), and the first and last (right; time baseline  $\approx 4$  min) from a random night (20130508)

of the errors in the SDSS reference positions.

### 2.1.13 Calibration Stability and Artifacts

#### Biases

Bias frames show variability on the short term, even from frame-to-frame in the same sequence. A difference of two contiguously taken raw biases immediately shows two types of artifacts. First, there is horizontal striping visible throughout a bias Mastercal image. This artifact is most severe in the left-most columns of cells in each OTA, and is attributed to clock synchronization when reading out each pixel row. This row to row variation is included in the cited read noise for ODI images. Second, in the bottom corners of each cell, there are diagonal features extending 70-80 pixels from the corner and has a maximum amplitude of about 30 counts. These features are co-located with the output amplifier glow, and indicate the presence of a short-term (of order of seconds) variation in the glow. Figure 2.12 shows the difference of two raw bias frames and presents examples of these artifacts. Both these artifacts affect final calibrated science images, but are mitigated by averaging many ( $\geq 10$ ) bias images into a master calibration file.

Over the longer term, biases show differences in the cell corners, in the area containing the output amplifier glow, as well as a large scale background level change. Figure 2.13 shows a sequence of six mastercal bias differences over time (a portion of OTA33). The sequence reads like a book, left to right on top, then left to right on the bottom. The images are the difference between the mastercal on an arbitrary day in early February, and a mastercal later on (in order: 1 day, 4 days, 11 days, 1 month, 2 months, 3 months).

Again, one notices the striped pattern on the left side of the OTA, known to be a quickly varying noise pattern. Some gradient differences are evident in individual cells starting with the very first image (1 day), and are obvious by the second image (4 days). Differences in the glow at the corners of the cells are present (at a low level) in the 1st image, with some larger differences (2 months; small green circles). There is also a dark vertical stripe along the left

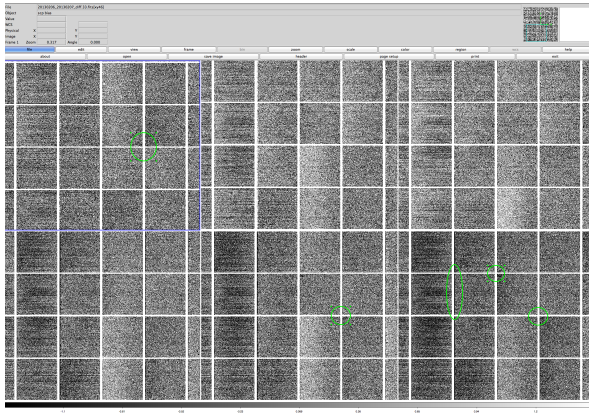


**Figure 2.13:** Mastercal bias differences for a portion of OTA33. In order (top left to right, bottom left to right): 1 day, 4 days, 11 days, 1 month, 2 months, 3 months. Zeroth day is 20130206.

edge of some cells (green ellipse in the 5th and 6th images).

## Darks

Darks also appear to vary on short timescales ( order of minutes). Figure 2.14 shows the differences of raw darks taken in the same sequence. The left-hand image is the difference of the first two darks in a sequence of 3, and the right-hand image is the difference of the first and last darks in a sequence. The images are more or less identical.

Again, two distinct types of artifacts are visible. The striping on the left side of the OTA is evident. Since these are raw darks (not bias subtracted) we can see that both the biases and the darks contribute to this artifact in the calibrated images. We also notice a diagonal artifact in the cell corners at the bottom of the cell. These are similar to the artifacts in the biases, though the artifacts in the dark are more pronounced. The artifacts extend over 100 pixels from the cell corner, and have an maximum amplitude of about -50 counts. These artifacts seem to form along the bottom edge of the transistor glow.

Like the biases, both these artifacts can affect the final calibrated science images, and are mitigated by averaging many dark images into the master calibration product.

Figure 2.15 shows a sequence of six mastercal dark differences over time (a portion of OTA33). The sequence reads like a book, left to right on top, then left to right on the bottom. The images are the difference between the mastercal on an arbitrary day in early February, and a mastercal later on (in order: 1 day, 4 days, 11 days, 1 month, 2 months, 3 months).

Differences at the cell corners (faint x's) are evident after only one day, and the overall dark level also evolves over a timescale of weeks to months. One can also see a portion of the circular pattern (dark bands that arc diagonally across the OTA) in images 3, 5, and 6, indicative of the position of the detector on the wafer when it was fabricated.

At three months, there is also a significant difference in the glow. Figure 2.16 is a rescaled

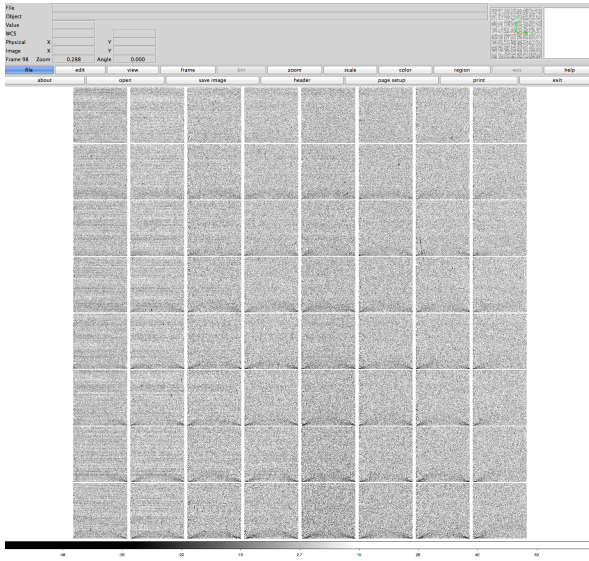


**Figure 2.14:** Difference between raw dark frames from the same sequence. 20130206.

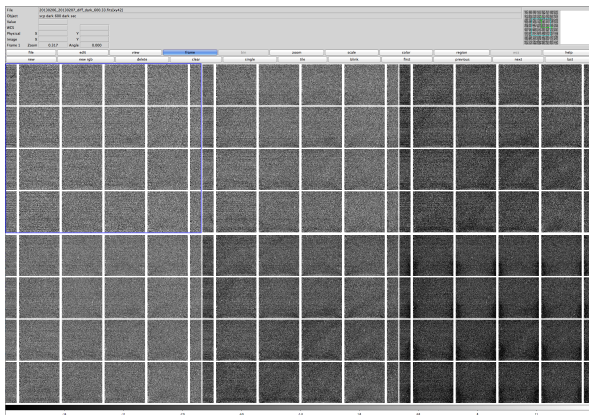


**Figure 2.15:** A sequence of mastercal dark differences over different time baselines (Top left to right: 1, 4, and 11 days; Bottom left to right: 1, 2 and 3 months).

version of the 6th image in the Figure 2.16 sequence. One can see that the entire region of the transistor glow is measurably different, by about 20 counts, or 10-15% of the brightest part of the glow.

The background also shows a drift over a period of weeks to months. There is no overall trend, as the background appears to bounce around, e.g. the difference is larger at 11 days, then smaller at 1 month. The difference between the Feb and May darks is about 1-15 counts.

Darks and biases are variable on short timescales (seconds to minutes). These lead to the diagonal „seagull” artifacts that can be seen in calibrated images, as well as the horizontal striping. Both biases and darks contain both these artifacts, as evidenced by the differences of raw images. For larger scale effects (i.e. background drift), the biases and darks seem to be stable on the timescale of 7-10 days. The combination of a greater number of frames in the mastercals also appears to smooth out some of the striping in the calibration image, resulting in partial mitigation of the striping in calibrated science images.

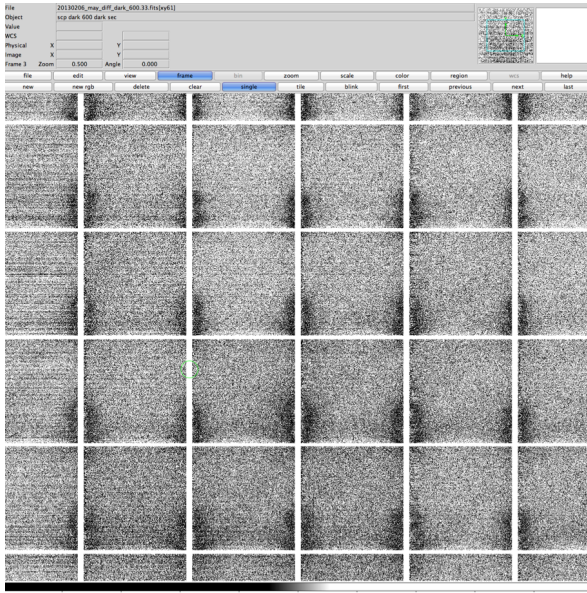


**Figure 2.16:** Difference in darks after 3 months, emphasizing the difference in glow. The difference in the glow is about 10-15% of the maximum glow level.

Some artifacts in bias and dark frames are attributed to the low light level CTE problem, as calibration products (bias, dark) contain bright features at the amplifiers. However, bias and dark images are taken under no background conditions whereas science images do contain a background sufficient to overcome the CTE problem, hence leading to some calibration uncertainties. This problem has been mitigated for the Lot 7 detectors in the 5x6 ODI focal plane.

## Dome Flats

Dome flats for the broadband filters appear to be exceptionally stable. Figure 2.17 shows mastercal differences for OTA33 with the r-band filter over a baseline of 1 day, 10 days, 1 month, 2 months, 3 months, 6 months, and 7 months (top left to right, middle left to right, bottom left). There are no striking artifacts, only some very minor large scale variations. The max amplitude of this variation at 7 months is about 1%. This might be due to changing illumination of the dflat screen as the lamps age, or are replaced.

For the z-band filter, there is a similar level of stability as the r-band filter. The ratio images for 1 day, 1 week, 1 month, 3 months, 6 months, and 8 months are shown in Fig. 2.18. Again we see some large scale variability starting at 6 months with an amplitude of 1%.

Dome flats for narrow-band (Mosaic) filters appear to be somewhat less stable and prone to artifacts due to light leaks. For Halpha, there are 4 ratios, shown in Fig. 2.19 (1 day, 1 month, 3 months and 8 months). There is significantly more variation in Halpha, with structure visible even at one day. There appears to be two components to the time instability in the Halpha dflats. First, some smaller scale structure (amplitude of 5% @ 1 day) can be seen. Oddly, this



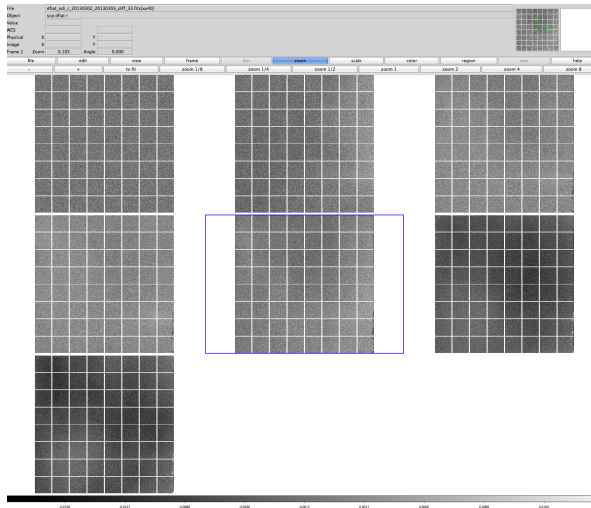


**Figure 2.17:** Mastercal ratios for a r-band dome flat over time periods of 1 day, 10 days, and 1, 2, 3, 6, and 7 months. Maximum variation is about 1%. This is OTA33.

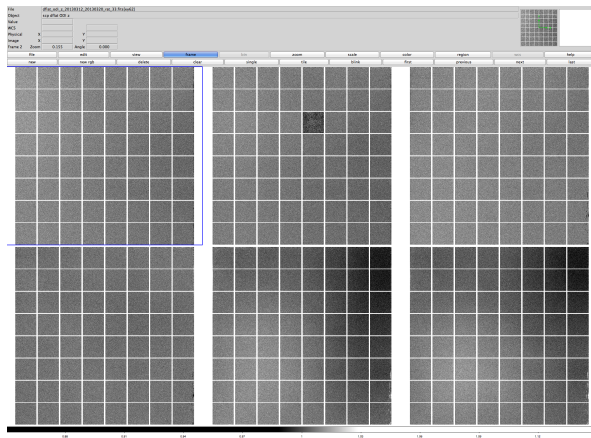


**Figure 2.18:** Mastercal ratios for a z-band dome flat over time periods of 1 day, 1 week, and 1, 3, and 6 months. Maximum variation is about 1%. This is OTA33.

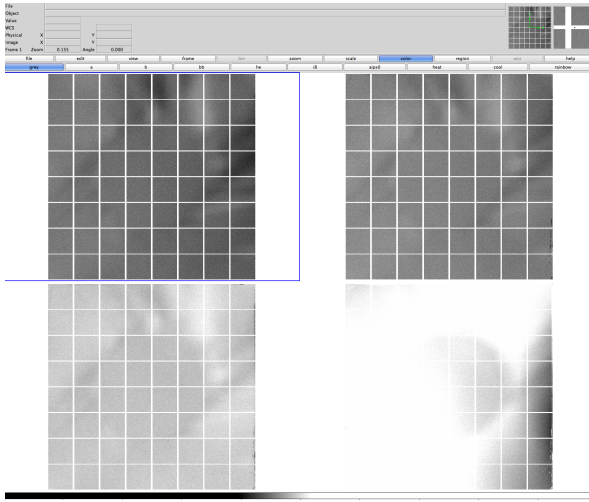


**Figure 2.19:** Mastercal differences for a Halpha dome flat over time frames of 1 day, 1 month, 3 months and 8 months. Maximum variation is about 5%. This is OTA33 with the Halpha filter (narrow-band, mosaic type filter).

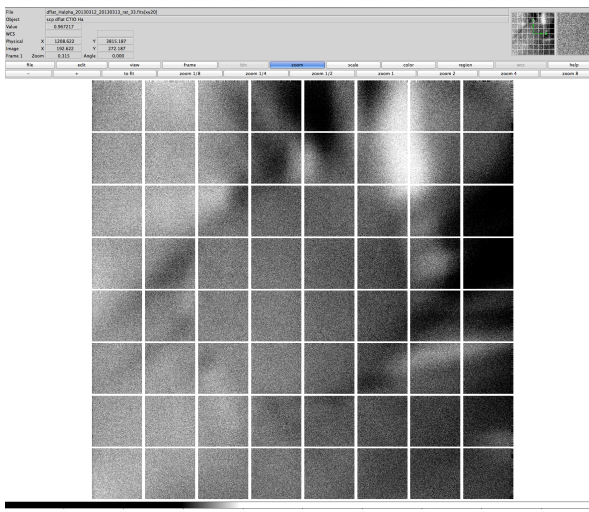


**Figure 2.20:** Mastercal ratio for a Halpha dome flat over a time period of a day. The contrast is stretched to enhance the structure. Maximum variation is about 5%. This is OTA33 with the Halpha filter (narrow-band, mosaic type filter).

component seems to be less of an effect at 3 and 8 months than 1 day. The second component is an overall background drift, which reaches about 3% over 8 months and can be seen as the brightening of the frame as a whole. The first component (short time scale, small spatial scale, large amplitude) has an interesting structure which is centered on OTA33, circular in the middle, with "arms" projecting radially outward. These artifacts are shown in detail in Fig. 2.20.

The acquisition schema for Mosaic filter flat fields has been changed late in semester 2014A : The clear glass inserts that facilitate guiding with ODI are obscured when dedicated dome or on-sky flat fields are taken. This will significantly reduce the effect of stray light and pupil ghost contribution to the flat fields. However, the effect on long-term stability has not been quantified yet.

## Chapter 3

# Observing with ODI

ODI has been designed to facilitate the following fundamental observing modes:

1. Snapshot observation — This is an unguided exposure. Telescope tracking performance limits this kind of exposure to 30 to 60 seconds before visible elongation of objects might affect image quality.
2. Telescope-guided observation — At least one OTA detector, preferably at the fringe of the detector array, is used to acquire a guide star signal. That guide star is used to derive a correction signal for the telescope guider, and long exposures without negative impact of tracking errors are feasible.

Note: Any detector used to acquire a guide star will have all amplifiers switched on during the exposure, and will thus be unavailable for science imaging due to amplifier glow.

3. Coherent OT Correction Imaging mode — This observing mode is an extension of Static Imaging where high-speed tip/tilt corrections are applied to the focal plane using the orthogonal transfer capability of the OTA detectors. This mode is only feasible if a minimum of three, or better four, guide stars are available. The guide star video will be used in two ways:
  - (a) To derive a slow averaged telescope guider correction signal (as in static imaging).
  - (b) To measure the coherent, fast average image motion and apply a correction for that image motion to the imaging part of the detector array using the OT shifting mode of the OTA detectors.

In this mode, the OT correction mode is effectively used to increase the bandwidth of the telescope guider by applying the high frequency component of the correction signal directly to the charge in the detectors.



Note: Any detector used to acquire a guide star will have all amplifiers switched on during the exposure, and will thus be unavailable for science imaging due to amplifier glow.

4. Local OT Correction Imaging mode — about four guide stars per OTA detector are used to correct for local (within a 2 arcmin radius) image motion as it is introduced by atmospheric turbulence. **This mode has been abandoned for ODI due to limitations of the OTA detector’s amplifier glow.**

### 3.1 Understanding the data flow in guided & OT corrected images

At the heart of any ODI observing mode involving the acquisition of guide stars is the Guide Core, which runs on `odiweb`. The Guide Core manages requesting the guide star readout from the Stargrasp CCD controllers, calculating centroids for guide stars, and forwarding the guide star stream to the OTAListener running on `wiyn-5`. If the coherent guide mode is active, the Guide Core will also calculate the common image motion and send OT shifting commands to the Stargrasp CCD controller.

The Guide Core is instantiated by the JBOSS application server on `odiweb` as part of the normal observing work flow. The Guide Core will receive a guide star configuration at each call of an individual exposure; the guide star configuration cannot be changed once an exposure is under way. A Guide star configuration can be defined either by:

1. Guide stars are manually selected in the OTAListener from a short exposure (“preimage”) taken before the main exposure.
2. Provided that the telescope pointing is sufficiently accurate, guide star candidates will be predicted from a catalog, skipping the requirement to obtain a preimage and manually selecting a guide star.

The OTAListener, running on `wiyn-5`, will display the guide stars videos and a history of their FWHM and flux. The guide star videos will also be forwarded to the Telescope Guider application, which by default runs on `wiyn-5` under control of the observer.

The Telescope Guider low-pass filters the motion of the guide stars and calculates a correction signal for the telescope. If selected by the user, a non-sidereal tracking vector can be injected into the calculation of the telescope guide signal. In this case the guide star will wander off in its video box.

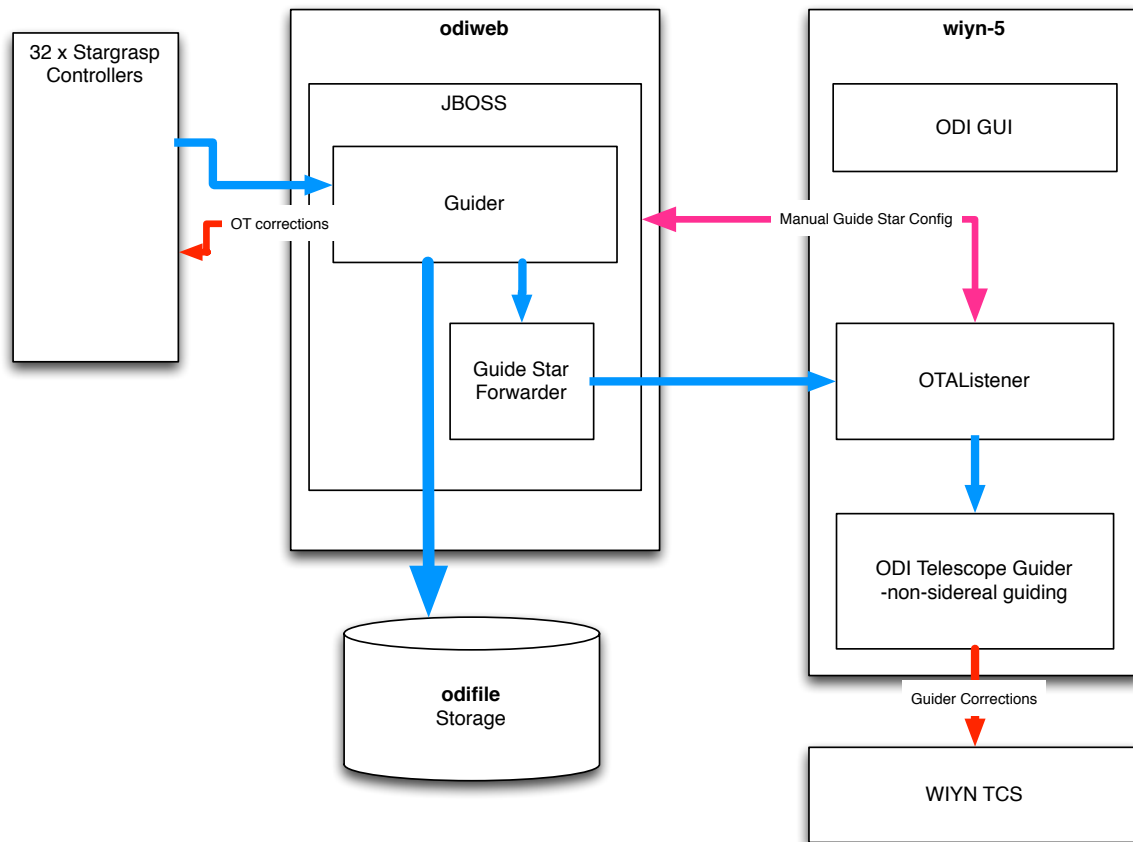


**Figure 3.1:** Flow of guide star video signal (blue arrows) from the Stargrasp CCD controller.

### 3.1.1 Open-Loop OT Correction vs. Closed-Loop Telescope Guidance

The telescope guider application sends commands to the telescope control system affecting the telescope drives, i.e., the entire image on the focal plane will drift (whereas the correction signals are designed to compensate a systematic drift). Since any telescope corrections are affecting the guide stars, from which the *slow, low-pass filtered* correction signals were derived, the Telescope Guider is a closed loop control system.

This, however, is not true for the OT corrections applied directly to the focal plane; while the image motion is sensed by the same guide stars used for telescope guiding, the fast, instantaneous correction is applied only to science image integrating cells, but not to the guide star acquiring cells. Therefore, the fast OT correction is operated using an open loop control system.

Since the fast OT correction does not feed back on the guide stars, the two telescope guider and OT corrector cannot work against each other. However, a poorly performing telescope guider would cause a significant oscillation of the telescope, which would then need correction



in the guide core.

## 3.2 Overview of ODI Tools

**Current State of ODI Observing** Observing with ODI is currently a mostly manual process, i.e., there is not much automation involved. Telescope pointing and focus changes are handled by the telescope operator. The filters are controlled by the observer, and the ADC setup is automated by the choice of the observer (do or do not use ADC). Guide stars for telescope tracking (and eventually OT shift corrections) are selected by the observer from a preimage. Since 2015, a guide star prediction mode is offered on a shared risk basis.

The observing station for ODI is `wiyn-5`, an eight core Mac Pro in the WIYN control room with two 30 inch LCD screens. The login information for `wiyn-5` is posted in the WIYN control room.

The following interfaces are typically needed to operate ODI as an observer:

1. The ODI Menu
2. For ODI Exposure Control:
  - (a) Filter configuration GUI.
  - (b) ODI Observation GUI.
  - (c) The OTAListener to handle the guide star workflow, but also to inspect images.
  - (d) Telescope Guider Interface.
  - (e) Optional: ADC status GUI
  - (f) Optional: Shutter status GUI
3. For inspecting ODI data:
  - (a) The ODI File Browser to browse and add comments to observed data products (images, biases, etc).
  - (b) A DS9 window to display individual OTA FITS images.
  - (c) An xterm window to work with IRAF.

## 3.3 The ODI Menu

The ODI Menu is the launch point for all ODI user interfaces. After login in at `wiyn-5` as `odiobserver`, start the ODI Menu using a shortcut on the desktop (see Fig. 3.2). All tools necessary for observing can be started from the launch menu.

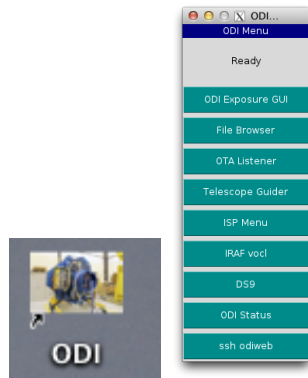


Figure 3.2: Launching the ODI Menu.

## 3.4 Launching Observations with the ODI GUI

The ODI GUI is the primary interface to start science observations with ODI. The GUI requires login with a user name and password<sup>1</sup>. Upon successful login, the observer sees the main GUI screen, where ODI observations are managed. Various instrument actions are accessible through different tabs: **Ad-hoc observing** for starting observations, **Dither Pattern** to create and manage dither patterns, **Instrument Control** to start and stop the CCD controller system, and **Dome Calibrations** to initiate pre-defined dome calibrations according to the ODI Standard Calibration Plan.

### 3.4.1 The Login Screen

While the primary purpose of the GUI is to provide a convenient mechanism to start ODI exposures, it is also a framework to ensure that meta-information about an observing run information is correctly captured.

While there is no high security mechanism deployed, the observer is required to login with a username and password into the observing system; the username is the email address of the PI; the password will be provided by the start of the observing run. Upon successful login, the observer can choose from observing programs he or she is affiliated with, see Fig. 3.3.

From an observer's point of view there is no incentive to login with a different user name or other than to a scheduled observing program. If an observer hacked into somebody else's account, the proprietary rights of such observations would be assigned to the hacked program, and the hacking observer would have to wait at least 18 months until data become publicly available.

---

<sup>1</sup>The login credentials will be provided to a scheduled observer

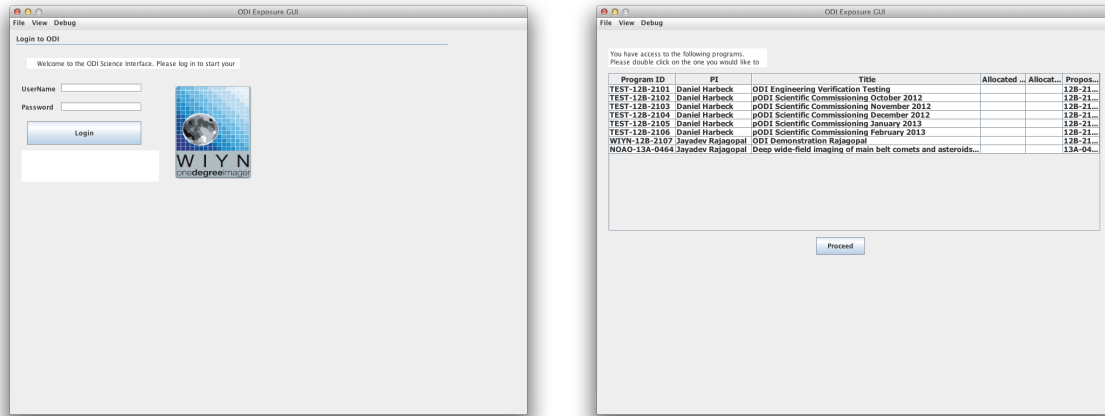


Figure 3.3: Login into the ODI GUI and selecting your program.

### 3.4.2 Ad hoc observations

The Ad hoc observation tab is the principal interface to initiate all major ODI observing. This tab is called “ad hoc observing” to distinguish it from a future mode in which nightly observation can be prepared in advance and managed for queue observing.

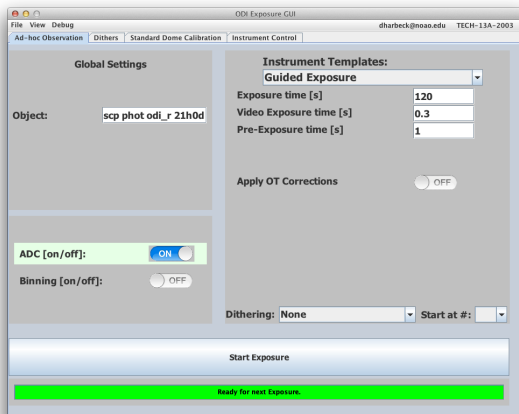


Figure 3.4: Ad-hoc observing tab: Enter the object name in the upper left, data acquisition parameters in the upper right, and start the exposure by pressing the *Start* button.

The general theme of the ad hoc observing mode is that on the left side of the tab the observer enters the Object name. On the right observation-specific *templates* are selected, where parameters such as exposure time are entered. Below the Object name the observer defines global parameters that will apply to most observations: Whether to use the atmospheric dispersion compensator (ADC) or if the science readout should be in binned mode (note that not all modes support these settings).

In the lower part of the ad hoc tab are located Start and Stop buttons to launch or interrupt



exposures, and an overall status display. The Stop button will end and readout the ongoing exposure, and interrupt an ongoing dither sequence.

The drop down menu on top of the *templates* section enables the observer to select different observing modes, such as bias, dark, flats, focus, and on-sky exposures. When selecting an observing mode, the template changes and displays only those parameters that are relevant for the actual mode. In the following we will go over the individual *templates*:

### Dome Calibration Templates

The endorsed way to create dome calibrations is using the Calibration tab, but it is also possible to manually invoke calibration observations:

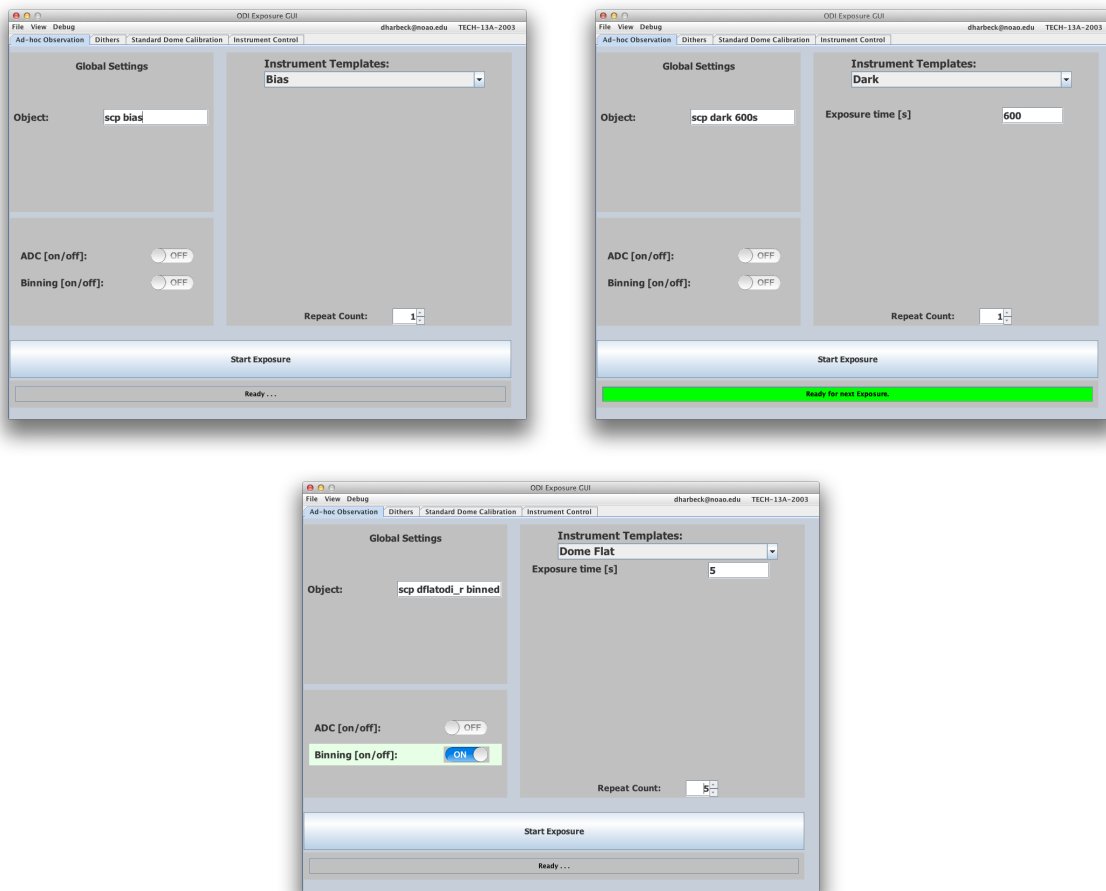


**Figure 3.5:** ODI observing templates for Bias, Dark, and Flat observations.

Figure 3.5 shows the three templates to initiate typical CCD calibration observations: Bias, Dark, and Flat observations.



**The Bias template** only has one parameter to enter, which is the number of bias frames to acquire.

The global ADC parameter is meaningless for a bias.

**The Dark template** has two parameters; the dark (exposure) time, and the number of repetitions of the dark. At this time we also want to introduce the concept of using a comma-separated list for exposure times: Exposure requests also accept a list of exposure times, which will then be executed in sequence. For example, if the exposure time entry for the dark exposure was given as “150,300,600”, the data acquisition system will take three dark images with dark times of 150s, 300s, and 600s, respectively.

The global ADC parameter is meaningless for a bias.

**The Dome Flat template** will initiate flat field observations. The parameter is the exposure time and the number of repetitions. The filter will be controlled separately in the filter GUI. Conceptually, a flat field observation is not really different from an unguided on-sky exposure; however, the file name prefix and OBSTYPE keywords in the resulting images will be set to properly identify the resulting data products as calibration flats.

**Note:** The ADC will be set into neutral position by the dome flat field template.

## On-Sky Observing Templates

The common theme for most on-sky ODI observing is the need to acquire a guide star, either to improve telescope guiding, or to apply on-chip tip/tilt image motion corrections using the orthogonal transfer capability of ODI. Accordingly the on-sky observing modes for ODI are distinguished by their use of guide stars. The two major modes are unguided observations that require no guide star acquisition, and guided observations that will acquire a guide star.

As of this writing, guide stars are always acquired through a short preimage for each observation from which the observer will manually select one or more guide stars. The guide star selection is handled by the guide star selection tool (the OTAListener). A mode to predict guide stars from a catalog is under development.

The two default on-sky exposures can be executed in the context of a dither sequence.

**Twilight Flat** The Twilight Flat (`tflat`) is conceptually identical to the dome flat template, however, it shall be invoked when acquiring flat fielding on the sky, either during twilight or during day time. Care should be taken when executing twilight flats as too long exposures can saturate the detectors and produce ghost charge in subsequent images.

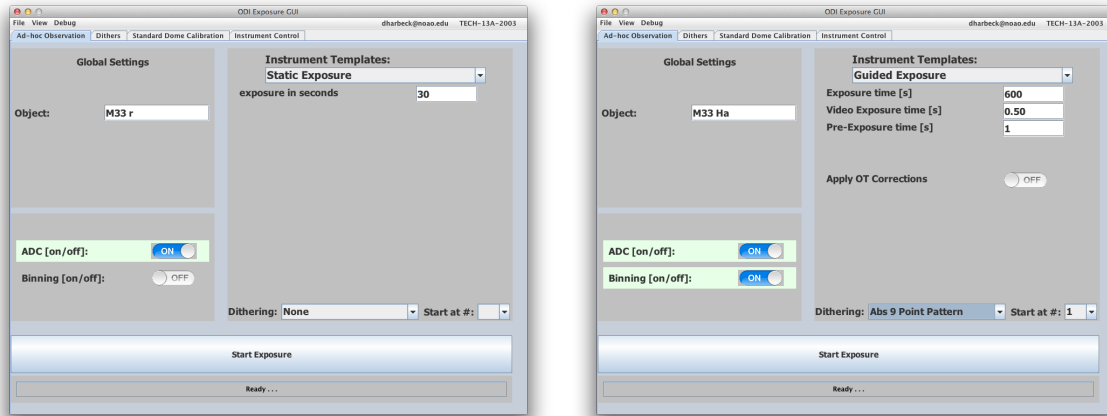


**Figure 3.6:** ODI default on-sky observing templates: Unguided Snapshot and Guided exposures.

When acquiring twilight flats, the ODI instrument rotator should be set to 0 degrees. If possible, the instrument should be in focus, and the telescope should be tracking sky (but not tracking rotation). Between individual flat fields, a 10" offset (in any direction) should be applied to allow for star rejection.

**Focus** The focus template will execute a classic focus sequence where multiple exposures at a different focus are collected in a single image. With each focus change, the telescope will be offset by a few arcseconds.

The inputs for the focus template are:

1. Exposure time for each focus step.
2. The *central* focus in the focus sequence.
3. The number of focus steps (an odd number).
4. The focus offset to be applied at each focus step.

The filter is controlled externally in the filter GUI. The global ADC and binning settings are currently ignored for the focus sequence.

**Unguided Observation** without a guide star requires the definition of the exposure time, and ADC mode. The filter is controlled externally in the filter GUI. If the observation should be done in a dither sequence, select a sequence at the bottom of the template.

**Note:** Due to limitations in WIYNs tracking performance, it is recommended to limit the exposure time for unguided exposures to less than 60 seconds.



**Guided Observation** The guided exposure will acquire guide stars from the focal plane and use those to (i) guide the telescope and (ii) if selected, apply a coherent image motion correction on the detector based on the average image motion of all guide stars.

The additional parameters are

1. The anticipated **video exposure time**. A good starting value for telescope guiding is 0.1s to 0.2s, whereas exposure times of 0.05s are useful for OT-based image motion compensation. Note, however, that the number of viable guide stars will dramatically decrease with shorter video exposure times. Due to limits in the CCD controller's firmware, the video exposure time cannot exceed 1 second. A reasonable lower limit for the guide star exposure time is about 0.01 seconds for a bright star.

**Note:** Currently, the video exposure time is determined at the point of starting an exposure sequence. A mode where the video exposure time will be adjusted based on the luminosity of the guide stars actually selected is in preparation.

**Note:** Due to the fat-zero issue, the faint end limitation of guide stars falls off faster than one would expect from photon statistics alone.

2. The **exposure time for the preimage** from which the guide stars will be selected. Consider that you must use the preimage to select guide stars that have to be bright enough for a 0.1s video exposure time or shorter. The preimage exposure time should hence be no longer than about ten times the video exposure time.

**Guide Conf from Preimage** This and the next template break down the “Guided Exposure” process into two steps. This template acquires a preimage and the observer can select guide stars. The guide star configuration will then be stored in the data acquisition and can be used later.

**Guided Exposure from Stored Guide Star Configuration** Once a guide star configuration has been stored in the data acquisition, this template will start using a guided exposure based on the stored guide stars, i.e., the observation will move on without a preimage.

This template is useful when the observing objective is to monitor the same field without dithering, e.g. for monitoring variable objects. Guide star positions will not be propagated with telescope moves, i.e., as soon as the telescope is repositioned, the stored guide star configuration will be rendered invalid (and possibly point to blank sky).

**Guided exposure with predicted Guide Stars** The predicted guide star mode uses a star catalog to select viable guide stars instead of a preimage. This mode is considered experimental at this time and should be used only after consultation with the start up personnel.

The input parameters are the ADC mode, exposure time and a dither pattern. The guide star prediction critically depends on the telescope pointing accuracy. There are two ways to ensure the pointing accuracy:

1. Use the pointing correction function in the OTAListener to adjust the telescope zero point.
2. Use the Startracker Camera ([Rajagopal et al., 2014](#)) to determine the actual pointing of the telescope (in contrast to the position reported by the telescope control system). This feature has been tested for  $40^\circ \leq \text{elevation} \leq 80^\circ$ . For elevations larger than  $80^\circ$  the WIYN dome can obscure the Startracker camera. At elevations  $\leq 40^\circ$ , toe-in of the telescope remains to be modeled in order for the Startracker camera to work accurately enough.

When using predicted guide stars, the guide star selection algorithm will attempt to select guide stars in all of the four outlying detectors. This allows for a wrongly predicted guide star in the ensemble. It is recommended to increase the guide star window size using OTAListener to minimize the risk of losing a guide star due to pointing inaccuracies. Note, however, that a larger guide window increases the risk of failed guide star acquisition due to hot pixel.

The ODI Guider should be directed to guide the telescope only on the brightest guide star. Check the according box in the **File** menu.

### 3.4.3 Standard Dome Calibrations

The dome calibrations as defined in ODI's standard calibration plan are coded in the "Standard Dome Calibration" tab. When starting calibration products in this tab, it will be ensured that they meet certain naming conventions, number of images, etc.

It is critically important to ensure that ODI's detectors have been powered on for **at least one hour** before acquiring standard calibration products.



Check those calibration products that are to be observed, and click the "Start Exposure" button. While it is possible to launch the entire set of afternoon calibrations with one click, it is recommended to split the calibration into three to four steps:

1. Bias and Darks. Launching the standard dark images will take 1/2 hour, and it might be helpful to separate the darks from the bias acquisition. The telescope setup for bias and darks is similar though; lights in the dome should be dark (note that the flat field lamps can be turned on with an intensity setting of "0"). Ten minutes before taking bias and darks no detectors must have been saturated, as otherwise residual charge could creep into the bias / dark calibration products.

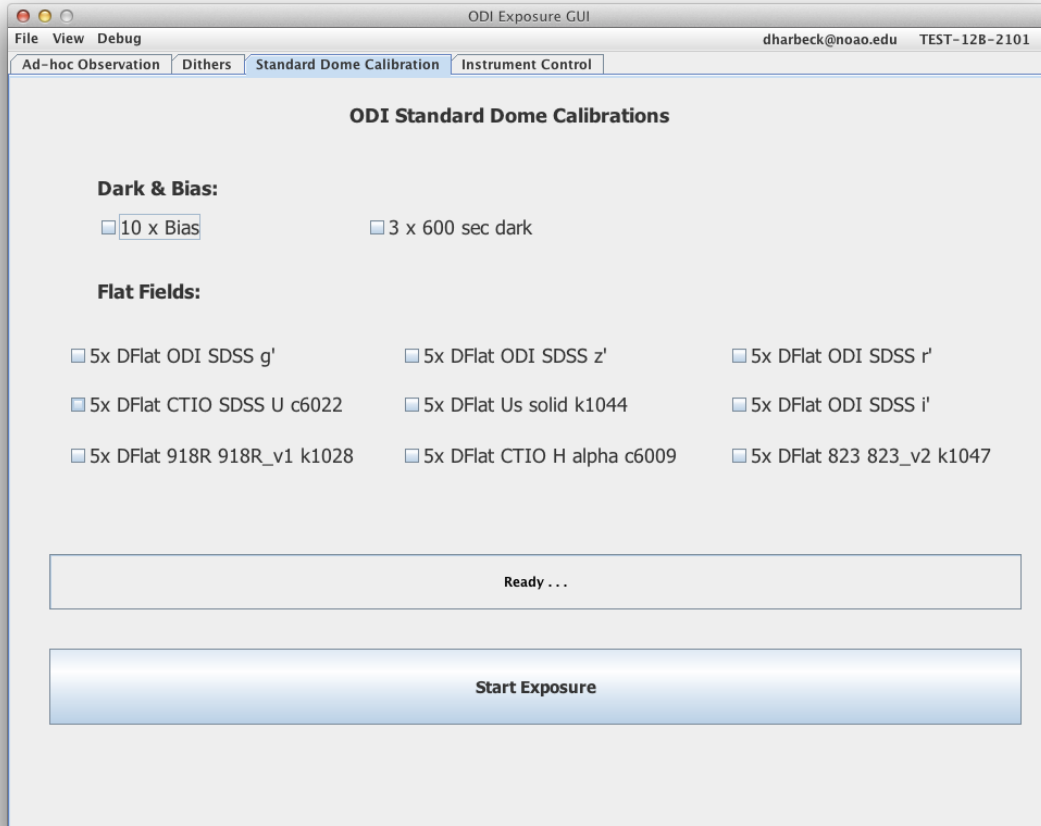


**Figure 3.7:** Standard Dome Calibration tab.

2. Dome flats for full size ODI filters; the requirement is that the dome lights are off, the telescope is pointed at the flat field screen, the mirror cover is open, and the flat field lamps are turned on (with intensity set to 0). The flat field lamp and exposure time will be configured automatically from a lookup table.
3. Dome flats for Mosaic size filters: It is not recommended that observers acquire flat fields with Mosaic filters, since stray light from the clear glass opening (to allow guide star acquisition) will invalidate the flat fields. Mosaic flat fields will be prepared by WIYN staff before and after an observing run, where the clear glass opening in the filter interface will be obscured, hence inhibiting any stray light.

A typical sequence for calibration could be: (i) acquire biases. (ii) acquire full size filter flats. (iii) acquire Mosaic filter flats. (iv) wait for 10 minutes, invoke a “CCD clean” in the instrument control tab, then start the darks, while going for dinner.

If dome flats are found to be inadequate, they should be flagged as such by using the commenting feature in the ODI File Browser.

### Note on binning

At this time, the Standard Calibration Tab only supports unbinned calibration products. Binned calibration products have to be obtained manually using the ad-hoc observing tab, while adhering to the standard calibration plan naming conventions.

### 3.4.4 Dither Patterns

TBD

## 3.5 Manual Filter & ADC Control

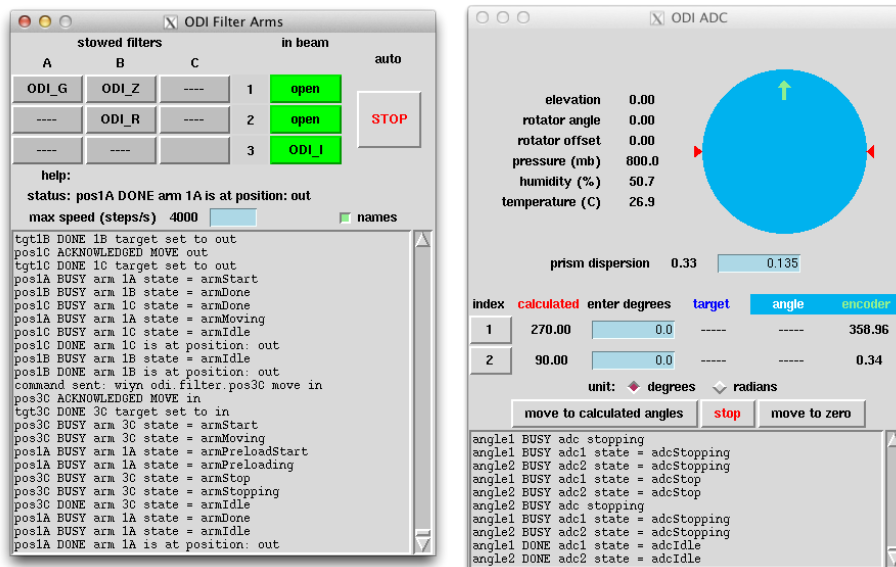


**Figure 3.8:** User interfaces to control the ODI filter arms (left) and the atmospheric dispersion compensator (right).

At this time, the ODI filter is controlled via a separate low-level engineering GUIs (see Fig. 3.8).



### 3.5.1 Filter Operation

The ODI filter mechanism consists of a total of nine filter arms that swing in and out of the beam. The filter arms are arranged in three layers (1 to 3, layer one is the closest to the telescope), on three posts (A through C). One filter per layer can be inserted into the beam at a time.

The GUI allows to slide filters into the beam, or stow them outside the beam. It is possible to have more than one filter in the beam if desired. The observer uses this interface to ensure the desired filter is in the beam.

### 3.5.2 ADC Operations

The ADC behavior is controlled in the Observing GUI, by either turning the ADC “on” or “off”. The ADC interface provides low-level access and monitoring capabilities.

The ADC consists of two rotating prisms, that, when aligned anti-parallel, cancel out each others’ dispersion and are in a *neutral* setting. This configuration can be reached by clicking on the “move to zero” button. This is the recommended setup for taking flat fields, or night exposures where ADC compensation is not desired. The latter might be the case for astrometric programs, where the rotating prism might introduce an extra, variable distortion.

It is undesirable to move the ADC prisms during an exposure, as stars in corner of the field of view would move on circles with a few pixels diameter, whereas stars in the center of the field of view would remain fixed. The practical impact would be that, while guiding the telescope using a guide star in the corner of the field of view, rotating the ADC prisms would lead to false guiding.

Hence when the ADC is set to “on” in the Observing GUI, the prisms’ orientation will be updated just before the start of each exposure

## 3.6 The ODI File Browser

The ODI File Browser is the visual ODI data management tool that solves the issue of having to deal with a complex image directory structure. It is possible to annotate images after they have been obtained, to preview images, and invoke several analysis tasks on an image (e.g., calculating its level, sending it to DS9, etc). The ODI File Browser operates solely on the file-system level, and can thus work with any local copy of valid raw ODI image directory.

The window of the ODI File Browser is divided into three major areas, and the workflow is oriented from the left to the right:



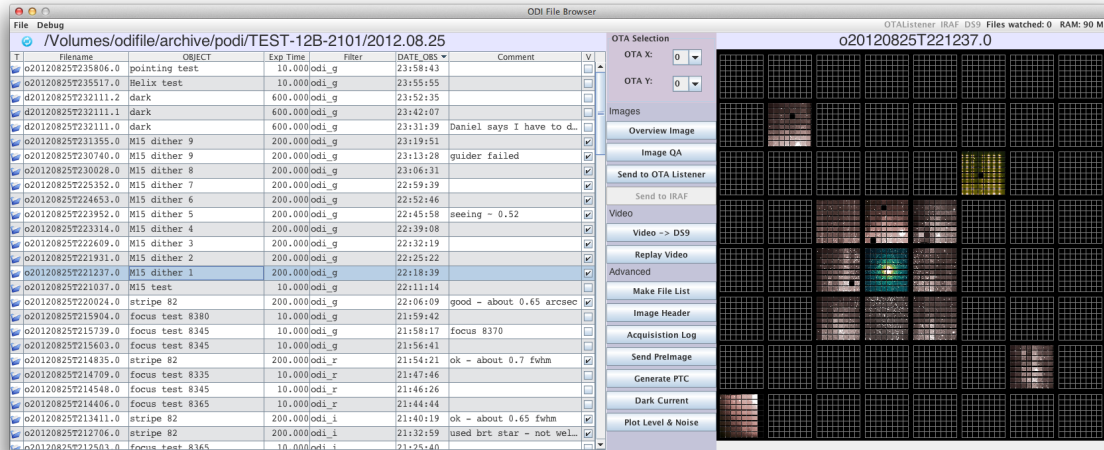


Figure 3.9: Screenshot of ODI File Browser

The **Image Directory Browser on the left** shows a listing of recognized ODI images in a storage directory. The list contains the image's data transfer status when available, the image name, the OBJECT header keyword, exposure time, filter, and DATE \_OBS header keywords. The *Comment field is user-editable*, i.e., the File Browser can be used like an observing sheet to annotate your observations. The File → Print Logsheets menu item will generate a latex file of the log-sheet to the file /tmp/pODILogfile.tex. If you are on a properly configured Mac with a late installation, a pdf file with the log sheet should automatically open. These log sheets will also contain additional information, such as telescope pointing, focus, etc.

The image listing can be sorted by each column, e.g., by exposure time. By default the table listing is sorted by the DATE-OBS keyword, with the latest image shown on top.

The File → Change Directory menu allows one to open a separate directory with ODI image sub-directories. When the dialog opens, note that you must select (not enter) the directory with the ODI image data. This might not be intuitive at the beginning.

Once a directory has been opened by the ODI File Browser, it will constantly be polled for the arrival of new image files. Thus, new exposures will automatically show up in the directory listing.

In the image listing, individual or groups of images are selectable.

The **center section** contains buttons to invoke actions on the selected ODI images. Since each ODI image consists of more than one FITS file, the OTA selection box on top of the buttons allows one to determine which FITS image on the 8x8 focal plane array is used for the action. Clicking on a button will invoke the actual action. You will find, however, that certain actions, such as displaying the image header, are executed when selecting a new file in the image listing automatically without needing to click the action button again.



In the **multi-use window on the right** we display the outcome of an image action. Its content will vary on your selected image action and can range from an overview image of the focal plane to more sophisticated detector analysis (although the expert functions will eventually disappear for the vanilla observatory system).

### 3.6.1 Image Actions and Image Display

**Overview Image** This action will display an overview image of the focal plane in the Multi use window at the right. The focal plane is represented by an 8x8 array of detectors that fit in the ODI focal plane, and each OTA detector is represented by a grid of its 8x8 cells (yes, there are two 8x8 grids in ODI, but they are of a different flavor). If data for a detector are available, the grid turns light grey, and if a preview-thumbnail image is present, it will be displayed.

The following actions can be done in this display:

1. Click left mouse button on an OTA image: This OTA detector is selected in the OTA Selection box in the center section.
2. Click right mouse button on an OTA image: This image will be sent to a DS9 display on the local computer, but will work only if (i) DS9 is actually open, and (ii) is connected to the SAMP hub as indicated in the menu bar.

When you scroll through the image list on the left, the overview image will automatically update as the data access speed allows.

**Send to OTAListener** When an instance of the OTAListener is running on the local machine, the selected image will be sent to the OTAListener.

**Send to IRAF (experimental)** When an IRAF vocl is running, and actually connected to the OTAListener, and you have the nfextern.odi package loaded, clicking this button will send the selected image to IRAF to be processed and displayed as a single image in DS9. Processing will take about 2-3 minutes, so be patient, and don't double click or launch another job until IRAF is done. As a reward, you can now use msexam on the entire image.

**Image Header** This Image action displays the first available main FITS header of an ODI image. When you scroll through the image list on the left, the image info window will automatically update as the data access speed allows.

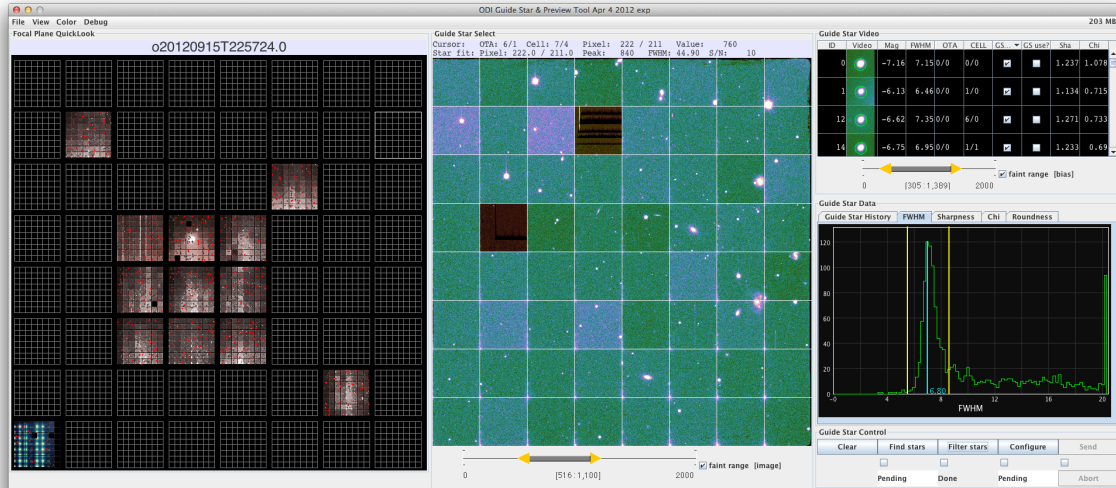


**Figure 3.10:** Screenshot of the OTAListener Application. An ODI image overview is shown at the left, and an individual OTA detector’s image is displayed in the center. To the right, either videos and a history chart of guide stars are shown, or statistics about bright, isolated stars in an image.

**Make File List** When interactively working with ODI images, the long and complex file names can be awkward to deal with. The Make File List tool allows you to select a set of images on the Image Browser on the left, and then generate a list of full path names for the FITS images in the right window. Cut and paste that list as you wish.

**Other functions:** These are specialized functions for detector characterization and are not discussed here. You might find the function “Plot Level & Noise” useful, as it displays the overscan level, overscan noise, image level, and image noise for all cells in the selected OTA of an image.

Note: In that view there is a bug where one needs to click radio buttons at the bottom of the window more than once to change between the different data views.

### 3.7 The OTAListener

The OTAListener is the Swiss-army knife for ODI image evaluations and guide star monitoring operations. It was initially written for the prototype camera QUOTA to passively *listen* in to the guide star video stream originating from the OTA detectors, and to display guide star videos for the observer’s peace of mind. During the QUOTA on-sky runs it became apparent that a tool to support the manual selection of guide stars would be critically required. The canonical place to put such a function was the guide star monitoring tool. Once the computer-

assisted guide star selection program was ready it turned out to be also a very fast ODI image browser. Driven by the ODI observing workflow, the OTAListener has grown substantially since the old QUOTA days and now combines several functions:

1. Display the guide star videos during an ongoing exposure, and show a timeline of quantities such as FWHM and flux for the guide stars.
2. Plot a radial profile of guide stars.
3. Support manual selection of guide stars from a preimage.
4. Support automatic detection of viable guide stars from a preimage.
5. Support automatic detection of isolated, bright stars in a regular image and calculate image quality metrics.
6. In the future to support automatic prediction of guide stars based on telescope pointing coordinates (not implemented in GUI yet).
7. Browse through an ODI image, and forward either individual OTA cells or entire OTA images to DS9.

The OTAListener's main window is divided into three main sections (see Fig. 3.10):

1. On the very left, an overview image of the entire ODI focal plane is shown. There you can click on an individual OTA to send it to the central image display. That overview image is functionally identical to the one in the ODI File Browser.
2. The central part of the OTAListener shows a single OTA image with its 64 cells. From that image, guide stars can be selected and added to a guide star candidate list on the right.
3. The right side displays guide stars. During an exposure, a video of the active guide stars is displayed, with a history strip chart below it. When guide star candidates are selected from a preimage, the guide star candidate catalog is visually represented here.

Furthermore, the OTAListener has a section to control the workflow for the guide star selection, and the ability to display statistics on a full image. We will come to that later.

**Limitations:** The OTAListener will not work with fz-compressed FITS images of such files. You will have to decompress the files before using them. Reading .fz compressed FITS images is a planned future upgrade.

### 3.7.1 Overview Image

The overview image on the left is very similar to the overview image in the ODI FileBrowser. The basic functions are:

1. Left-click on an OTA: That OTA will be displayed in the center single OTA image viewer.
2. Right-click on an OTA: That OTA image will be displayed in DS9, when running.

### 3.7.2 Single OTA Display & Guide Star Selection

The central image display can be used to either inspect an OTA image in detail, or to pick guide stars. Whenever the mouse is moving over the image display the OTAListener will attempt to centroid on a star at the mouse location. If there is an isolated bright star present, a green circle will appear around the best fitted location of that star. When you left-click while a star is identified it will be added to the image catalog on the right as a viable guide star.

On top of the image we display image information at the position of the mouse: The first line contains raw image information, while the second line presents statistics about the fit of a star.

**Image contrast:** The contrast setting of the image can be adjusted by the slider below the image. The selection in that slider is equivalent to the z1 and z2 settings when you display FITS images in IRAF. When you check the "faint" box, the slider range will be modified from 0 to 2000 instead of the full dynamic range of the image.

Notes:

1. The dynamical range only changes when the sliders are released; the image display will not update until then.
2. For the OTA display each cell becomes overscan corrected, and the pedestal level is set to 100 ADUs.

### 3.7.3 Correcting the Telescope Pointing Zero Point

After large slews, the WIYN telescope can have significant pointing uncertainties, where deviation up to 8' have been reported. Traditionally, operators have been slewing first to a nearby bright star and corrected the pointing of WIYN there, and only then moved to the



final target. This is impractical for ODI where the telescope's bore sight coincides with a gap between detectors.

The OTAListener has the build-in mechanism to correct the telescope pointing by matching stars in an image with a catalog, determining the offset in RA and Dec as well as in instrument rotation, and to issue a offset correction to the telescope control system. The work flow in practice is:

1. When focused, take a 60 second image at the location where the telescope pointing is to be corrected. Display in OTAListener.
2. In the menu, select **Pointing** → **Pointing Offset**. The program will first search for stars in the image and then match with a star catalog. The result of the match will be displayed in a dialog box, indicating offsets in RA, Dec, and rotation, and indicates how many stars were involved in the match and what the error of the solution is.
3. If the result is plausible ( $\text{rms} \leq 1''$ , more than 15 stars matched, and the rotation  $\approx 1^\circ \pm 0.2^\circ$ ), answer the question if the offset should be applied with "yes". The Ra and Dec offset will be used to adjust the telescope pointing. The rotation offset will be stored in the OTAListener for future use.

**Warning: A telescope pointing correction must only be applied when the position offset of the telescope is 0/0.**

4. If the pointing correction is not applied, the RA, Dec, and rotation corrections will be stored within the OTAListener for future reference.

### 3.8 Telescope Guider Application

Lacking any external guider capabilities on the ODI telescope port, ODI has to provide a telescope guider signal, and a guide star stream that is forwarded by the OTAListener to a dedicated telescope guider application. The upper part of the application's window includes a representation of the current mean position of the guide stars relative to their initial positions, a history of deviations in the X and Y pixel direction, and a power spectrum of the guide star signal (for your information only at this time).

The status display in the middle of the guider application shows:

1. If a connection to the WIYN router is available.
2. If a connection to a guide star source is established.
3. The state of the guider engine.

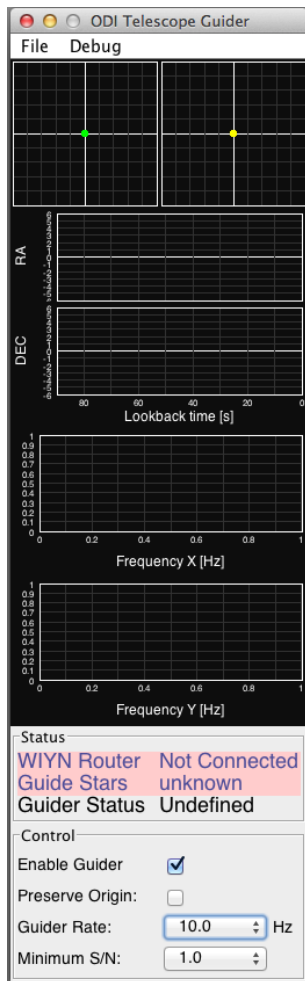


**Figure 3.11:** Screen shot of pODI telescope guider interface



The guider engine state can be undefined, exposure started but waiting for shutter to open, locking on guide stars initial positions, guiding, guide star lost, or idle.

The observer can define if the guider should forward a correction signal to the WIYN telescope control system, and at which rate such a signal is to be sent (the guider will average the current location in the meantime). Also, a minimum signal to noise ratio for the guide stars can be specified. The S/N defines the threshold for valid guide stars and drives (i) when the guider thinks that the shutter has been opened, and (ii) when the guider assumes that guide stars are lost.

A special flag (preserve origin) will bypass the process of finding a new initial position for a new exposure, but will use the stored initial positions of the guide stars from the last exposure instead. This is useful to force a series of exposures to have the same position on sky when the guide star configuration is not changed. This special mode can be useful since ODI will lose sight of the guide stars when the shutter closes, and only during the next exposure the guide stars will appear again. In the meantime, though, the telescope might have slightly drifted away.

### 3.8.1 Non-sidereal tracking

Non-sidereal tracking is possible with ODI and is handled by the ODI Telescope Guider application. Non-sidereal tracking is implemented by adding an additional time-dependent offset to the telescope tracking corrections. Hence, applying non-sidereal tracking corrections requires the execution of a guided exposure.

To enable non-sidereal tracking, click on “Non-sidereal tracking” in the File menu. To disable non-sidereal tracking, click the same menu entry again, or enter zero as the drift rates.

Once the non-sidereal tracking mode is enabled, an entry field for the slew rate will appear at the bottom of the Guider window; as soon as a tracking rate is entered. The non-sidereal slew rate is entered as arcseconds / hour in the RA and Dec directions.

As the telescope will drift during an exposure with respect to the stellar background, a guide star will also move and eventually drift out of its guide window. To avoid losing the guide star it is advisable to:

1. Make sure that the maximum slew rate  $\times$  exposure time is smaller than  $1/3$  of the guide star window size.
2. Select a large guide star window size in the OTAListener’s “Guide Stars” menu.

In a future upgrade it is planned to allow the guide star readout window to follow the guide star as it moves during an exposure. In that case, the maximum useful exposure time will be





limited by the distance of the guide star to the border of an OTA cell in the direction of the slew vector.

### 3.9 Where are My Data?

ODI data are stored locally on a large file server (`odifile`). Immediately after an ODI exposure is completed, data will be transferred via the Internet to the **ODI Pipeline, Portal, and Archive (PPA)**, which is hosted at the University of Indiana. Under normal circumstances, raw data should be ingested at PPA within minutes, albeit data transfer issues can delay the availability of individual exposures. Such issues should be resolved within one business day.

The preferred method to access your **raw** data is to download them from PPA once you are back at your home institution. The portal can be reached at

<http://portal.odi.iu.edu/>

Should there be a need for immediate access to your data, it is possible to attach a USB drive to `wiyn-5` and copy data directly to your drive. Your data will be located at:

```
/mnt/odiweb/archive/5odi/YOUR_PROGRAM_ID/DATE_OF_NIGHT
```

`YOUR_PROGRAM_ID` refers to the identifier of your observing run, which consists of four letters indicating your time granting institution, followed by the semester, and the proposal number, e.g., INDI-13A-0435.

`DATE_OF_NIGHT` refers to the date of the evening your observations (in Mountain Time) started, i.e, the date identified for the directory will not roll over at midnight.

**Note:** Due to the large data volume it is not acceptable to transfer data from the ODI data acquisition system (or any computer at WIYN) directly to your home institution or anywhere else, as the charged for the data transfer from the mountain is metered and charged to WIYN.

#### 3.9.1 Quick Reduce Data

A quick-reduce pipeline is installed on the ODI data acquisition system, and it can be invoked in the ODI File Browser to facilitate fast assesment of the data. This pipeline is configured to write output data to

```
/mnt/odiscratch/qr
```



The quickreduce pipeline is the formally supported calibration software for the WIYN One degree Imager. The source code is hosted on github: <https://github.com/WIYN-ODI/QuickReduce>. Documentation is available at the author's home page: <http://members.galev.org/rkotulla/research/podi-pipeline/>. Please note that the support focus for quickreduce is the use within the observatory and the PPA system.

### 3.9.2 Obtaining help

For any help with your data after completion of your observation, please refer to <https://groups.google.com/forum/#!forum/odi-ppa-help>

## Chapter 4

# ODI Observing Strategies & Hints

### 4.1 Starting to Observe: A Walkthrough

*This section is a rewrite of Marla Geha's observing notes.*

#### 4.1.1 Afternoon

In the winter, plan to arrive no later than 3pm in the WIYN control room. During the summer, start of ODI care-taking can start later. WIYN or KPNO personnel will turn on the power supplies (“Agilents”) for the CCD Controllers. During the first day of your run, this will be covered by your startup person. For the subsequent nights, arrange with your telescope operator that somebody will turn on the Agilents the next day.

Once the power supplies are powered on, execute the following sequence in the Observing GUI's “Instrument Control” panel<sup>1</sup>:

1. SG warm start
2. CCD Pon
3. CCD Poff
4. CCD Pon
5. CCD Clean
6. CCD Calibrate

---

<sup>1</sup>Editor's comment: Refer to document ODI-PROC-0006, “ODI Start and End of Observing Procedure” for an up to date instructions.

Then, take one test bias using the “Ad Hoc Observing” panel in the Observing GUI. Set the “OBJECT” field for this bias to “Test bias after pon”. If this looks bad (see section on bad images in this manual) do a second CCD Clean and another bias. If problems persist, ask for support.

Now follow a very important step before you can acquire afternoon calibrations:



WAIT 30 MINUTES.

Once waiting has completed (the temperature of the focal plane has stabilized now), the telescope operator has probably arrived (around 4pm). Once the telescope operator has made sure the telescope is ready to take calibrations, go ahead:

**Flats:** Take dome flats in the filters which will be used during the night. There is a table providing the lamp level and exposure time for each filter in this manual (Table. 4.1), but we will use the Standard Dome Calibration tab in the GUI to launch flats. Ask the operator if the telescope is ready for flat fields. We will take one test flat field using the “Ad hoc” tab first; any ODI griz filter will suffice. Ask the operator to turn on the flat field lamp with the appropriate intensity. Take a single dome flat in the and ensure it is correct (e.g., the tertiary could be pointing to a different port). Then go ahead and take all the dome flats you need, using the Dome Calibration Tab in the GUI.

**Bias:** Use ‘Standard Calibration’ window to take 10x bias.

**Dark:** Use ‘Standard Calibration’ window to take 3x600s darks. Make sure the dome is dark with mirror covers closed. You might want to start the darks just before leaving for dinner. If the darks will finish the dome calibrations, you might want to inform the observing assistant that the dome can be opened as soon as the darks have finished.

#### 4.1.2 Evening

**Focus:** After opening the dome, ask the operator to move to the first target field and set focus value to roughly that of the previous night. The first field will probably be a photometric standard calibration field. Under „Ad hoc” observing, select „Initial focus exposure” from templates (need to scroll to bottom). Set values as: exp time  $\sim 5s$ , center focus = whatever you think is a good starting point (8900 focus units in the winter in the full size filters) set, # of exp = 5, size = 50. Take image. When its done, display in ds9 (double click). Use `imexam (r)` to determine best value. First focus value is at top, last is on bottom. Repeat focus sequence with step size =25. Once you know the focus, ask the operator to move the



telescope focus there. Since the focus sequence does not restore telescope pointing offsets, ask the operator to restore the offsets to where you want them to be.

**Science exposure:** Go to pointing star near field. The field center is in between CCD gaps, so hope to see glow of the bright stars. Move to field. Ask for an offset of '240 240' to bring field center to center of ODI.

Decide on dither pattern. There is 'canned' pattern to cover all CCD and cell gaps. Some people might want to create their own pattern, e.g. to only cover the cell gaps (x=0,15,10,-10,-15, y=0,15,-10,-10,15).

Set the exposure time and video exposure time. For clear, stable nights, set video exposure time to 0.2s. For less than optimum nights with clouds, set to 0.5s. Your strategy might vary if you want to apply OT corrections (not recommended yet), or a field lacks bright stars.

Hit expose and wait a few seconds. There will be a double beep and an image will appear in the OTAListener; now you need to select a guide star from the preimage. Click on bright stars to find a suitable bright guide star. Try flanking CCDs first. If star is 'OK' or 'faint', the Guide Star Video box will show a green check mark. Click on 'Use?' and then click towards bottom 'Expose with a Guide Star'. If you cannot find a good guide star, click on blank sky and move ahead with that "guide star". Disable the telescope guider, or abort the exposure once the shutter has opened.

For images that are finished, one can click and hit 'Quick reduce to DS9' which does exactly that in about 20 seconds. Inspect the image as needed in DS9.

During the exposure, watch FWHM of guide star. You can tweak the focus by  $\pm 20$  steps to see if image quality improves.

## 4.2 Guide Star Selection

For a guide star exposure time of 0.1s the recommended guide star magnitude (instrumental as indicated by the OTAListener) is brighter than -14 mag; ideally -16 mag. Telescope guiding will work with fainter stars, but there is no room for clouds in that case.

### 4.2.1 Automatic Guide Star Selection

Predictive guide star selection works for full-size filters only at this time. Mosaic filters are not supported yet!

Predictive guide star selection chooses guide stars based on



1. The current Telescope pointing
2. The World coordinate solution of the focal plane
3. An input catalogue of bright stars.

Errors in any one of the three factors above will disable the ability to correctly predict guide stars. Keeping track of the telescope pointing is the most critical limiting factor when using predictive guide star selection at the WIYN telescope.

To use predictive guide star selection:

1. After a slew to your target and focusing, ask the operator to use the Startracker camera to correct the telescope pointing.
2. Set the guide star window size to 128 pixels in the OTAListener.  
This will increase the search window for a guide star and improve the chances of locking onto a star, even if the telescope pointing has drifted slightly.
3. Take a 30 second unguided image and use the OTAListener to determine the pointing offset.  
**DO NOT apply the pointing offset to the TCS.** The pointing offset will now be stored internally in the OTAListener and will be displayed in the upper right corner of the Menu bar.
4. In the OTAListener, under the Telescope Pointing menu, enable automatic pointing measurement.
5. Start your observation sequence using the "Proto GS Predicted Exposure" template in the Exposure GUI.
  - (a) Choose a video exposure time of about 0.3 sec in r,i, or 0.5 sec in g,z.
  - (b) Monitor the guide star videos to ensure that the guide star prediction worked.
  - (c) Monitor and adjust the image focus on-the-fly, if necessary.

Notes:

1. The OTAListener will use the internally stored telescope pointing offset and the telescope pointing at the time of the guide star request to map star catalogue positions to pixels.
2. Whenever a new image is loaded into the OTAListener, the pointing offset is recalculated and to be used subsequently. Hence, DO NOT load an old image into the OTAListener while executing an observing sequence that depends on predicted guide stars.



3. When using predicted guide stars, it is recommended to check the "Guide on brightest star only" feature in the ODI Telescope Guider File menu. Albeit by default up to four guide stars are active, a guide catalog-predicted guide star may not be present, be unusable, etc.
4. There seems to be a bug in the telescope guider application where the initial locking of the guide stars does not succeed if one guide star is absent / too faint. In that case, select the "Restart guiding" option in the Guider's File menu.

### 4.3 Exposure Time Calculator

Refer to exposure time calculator: <http://www.wiyn.org/ODI/Observe/wiynodietc.html>.

### 4.4 Dithering

Dither patterns can be defined by the observer using the Observing GUI. A 9-point dither pattern will be predefined from within the ODI Exposure GUI. Recommended patterns are:

- To fill the gaps between OTA cells:  
Three point pattern 0/0 20/-10 -10/-20 in arc seconds
- To optimize for homogeneous coverage: Nine point pattern stored in observing GUI.
- To achieve reasonable coverage with fewer dither positions:  
7 point: 0/0 158/-47 107/213 53/177 -154/ 54 -205/ -98 -46/-208  
5 point: 0/0 156/-52 51/159 -214/108 -51/-103

### 4.5 Telescope Guiding & OT Corrections

The WIYN telescope does not track very well, and it is a general recommendation to use a guide star for exposure times longer than 60 seconds. Even if the coherent OT correction mode is used, it is advisable to enable the telescope guider. While the OT corrections will diligently compensate any systematic drift of the telescope, the drift will cause (i) the guide stars to wander out of their readout box, and (ii) the imaging area to be reduced as the charge image is driven out of the detector area.

## 4.6 Filters

There are four native full-size filters available for ODI: SDSS g', SDSS r', SDSS i', and SDSS z'. Due to some passband variations from the original specification we refer to these filters as ODI g',r',i, and z'. The most significant difference is in the ODI z' band filter, which has a red cutoff in contrast to the SDSS z' band filter. Due to the falloff of the CCD response in the red, this has the advantage of a controlled red cut off of the filter.

In addition to the full size ODI filters it is possible to mount most Mosaic camera filters in ODI via a special adapter. This adapter has clear glass inserts over the outer detectors to allow guide star acquisition, and the central array is covered by the Mosaic filter.

The clear glass inserts make the central imaging area susceptible to stray light, which shows most dramatically in dome flat fields. The stray light issue is aggravated for blue filters by the red color of the flat field lamps. For flat field acquisition, the clear glass inserts must be covered to avoid the stray light. Mosaic flat fields are hence not recommended to be acquired by observers, but will be provided by WIYN staff.

The transmission curves of the ODI Filters and all Kitt Peak / CTIO Mosaic filters are included in the ODI Exposure Time Calculator. Please refer to the ETC for the actual system throughput in each filter.

Table 4.1 lists the recommended flat field settings and focus offsets for filters that have been operated in ODI.

## 4.7 Pointing offsets for ODI

ODI's imaging field of view is slightly off-centered with respect to WIYN's optical axis. The optical axis is in the void between the detectors OTA 33, OTA 34, OTA 43, and OTA 44. To center a pointing on detector OTA 33, i.e., the center of the  $3 \times 3$  science field of view, use the

**standard offset 240" E, 240" N.**

### 4.7.1 Correcting Telescope Pointing using ODI

After a large slew, WIYN's absolute pointing can have an error of up to 4 arc minutes. For other instruments at WIYN it has been usual practice to point to a nearby bright star, adjust the pointing, and then locally slew the telescope to its final destination. This approach, however, was not feasible before with pODI.

The OTAListener implements a similar, but automated strategy: With an image loaded, the function at the menu *Pointing*  $\rightarrow$  *Telescope Offset* will match stars in the loaded image



Name	ID	FF High	T <sub>exp</sub>	Counts	Focus Offset	Comment
ODI u'	w106	3200	25		+30	
ODI g'	w104	1900	5	28000	0	
ODI r'	w105	1300	4	29000	<b>0</b>	<b>focus reference</b>
ODI i'	w103	1000	5	33000	0	
ODI z'	w101	1000	5	30000	0	
ODI NB695	w107	2500	3	30000	0	
U solid	k1044	3200	25 <sup>2</sup>		+35	
CTIO H <sub>α</sub>	c6009	2500	4 <sup>2</sup>	30000	+40 ± 10	
CTIO SII	c6013	2500	4	30000		
CTIO O[III]	c6014	3200	10	32000	+40	<sup>1</sup>
CTIO O[II]		3200	240	2000	+40	
CTIO u'	c6022	3200	8	20000	+50 ± 10	<sup>1</sup>
WRC3	k1021	3200	10			<sup>1</sup>
918R v1	k1028	2000	6	30000	+35	
815	k1026	2000	6	3000	+66 ± 20	
823 v2	k1047	2000	5	27000	0 ± 15	
BATC 390	k1052	3200	15	29000	+ 30	
BATC 420	k1053	3200	8	28000	+60	
Open	n/a				-290 ± 20	

**Table 4.1:** ODI filter properties for conventional flat fielding. Exposure times for binned flat fields shall be divided by 2.

Notes: <sup>1</sup> — Stray light warning: dome flats are severely affected by stray light. Sky flats are recommended. <sup>2</sup> Recommendation for clear glass inserts covered.

with a catalog and determine the pointing offset. The observer has then the choice to adjust the telescope's zero point setting, i.e., move the telescope to where it thinks it is actually pointing. This is the equivalent of using a hand paddle to adjust the telescope position. When successful, the WCS typical RMS is of order of 0.3" to  $\leq 1$ ". Only then should a WCS offset be accepted. The observer can select if to apply a correction to the telescope pointing. If rejected, the OTAListener will store the pointing correction for future use. If accepted, the telescope pointing correction held in the OTAListener will be set to zero, and the next exposures should be correctly pointed.

In practice, correcting the telescope pointing should be used when (i) the pointing of the telescope is crucial for the success of the observing run, or (ii) a faint object with known RA/Dec needs to be identified in an image, e.g., before committing to a long exposure.

Since WIYN's pointing will drift when not guided, the pointing correction will deviate over time, and becomes invalid after a major slew.

Name	FF High	T <sub>exp</sub>
odi u'	n/a	n/a s
odi g'	2800	0.8 s
odi r'	1800	1 s
odi i'	1500	1 s
odi z'	1500	1 s
odi NB695'	3200	1 s

**Table 4.2:** Flat field exposure times for use with slow shutter speeds (vm 500). Those shutter speeds allow for ghost suppression.

## 4.8 Observing Overheads

Execution times for instrument operations that are in addition to the exposure time (“overhead”) are listed in table 4.3.

Operation	Execution Time	Comments
Detector Operations		
Bias, Flat, Unguided Exposure	30 sec	Includes detector cleaning and meta-data generation after exposure.
Guided exposure	60 +20 sec	Includes overhead for preimage acquisition, final image readout, and an estimated 20 sec to pick a guide star
Guided exposure from prediction	30 sec	Guide stars are selected from catalog instead of from preimage. Experimental mode.
Instrument Operations		
Filter change	20 sec	When filters are in different layers
	40 sec	When filters are in same layer
ADC setup	30 seconds	Initial setup
	≤ 10sec	Incremental setup

**Table 4.3:** Overheads for exposures. Add the actual exposure time to get the total execution time.

## Chapter 5

# Afternoon Calibrations and the ODI Standard Calibration Plan

To ensure the quality of data that are calibrated under the auspices of the PPA, a *standard calibration plan* for ODI has been defined that each observer is required to adhere to.

It entails afternoon calibration products to be taken in the dome (bias, dome flats, sky flats, and dark exposures), as well as photometric calibration exposures in all SDSS broad band filters that are mounted in ODI. Observers familiar with CCD imagers should already be familiar with the listed calibration products.

Standard calibration products are identified by a prefix “scp” in the OBJECT name, followed by the type of calibration. This results in the following convention to fill in the OBJECT fields for standard calibration products:

- Bias observations: *scp bias*.
- Dark observations: *scp dark xxx sec*, where xxx is the dark time.
- Dome flat observations: *scp dflat filterName*, where filterName is the name of the filter in the beam.
- Sky flat observations: *scp tflat filterName*, where filterName is the name of the filter in the beam.
- Photometric calibration fields: *scp phot fieldName filterName*, where fieldName is the name of the calibration field, and filterName is the name of the filter in the beam.

## 5.1 Summary of standard calibration plan observations

The current standard calibration plan products are:

Afternoon calibration:

1.  $5 \times$  dome flats at an exposure level of about 30000 ADCs in all filters that are to be used that night. In order to efficiently suppress the ODI pupil ghost, the shutter will be operated in a special slow mode. This mode is only usable by observatory staff, and hence observers will usually not acquire any flat fields.
2.  $10 \times$  bias exposures.
3.  $3 \times 600$  second dark exposures

Night-time calibration:

1. At least one set within the first 3 hours of a night of photometric standard field observations in all full-sized ODI filters. One set of photometric exposures consists of **60 second exposures in each of the ODI g r i z filters**. Viable calibration fields have been chosen to have (i) SDSS coverage and additional, high-precision coverage either by the SDSS Stripe 82 or PanSTARRS Photometric Reference Ladder ([Magnier et al., 2013](#)):

R.A.	Dec.	Reference
23h	0 deg	Stripe 82
24h	0 deg	Stripe 82
1h	0 deg	Stripe 82
2h	0 deg	Stripe 82
4h	0 deg	SDSS
6h	0 deg	SDSS
8h	0 deg	SDSS
12h	+25 deg	PanSTARRS Photometric Reference Ladder, SDSS
17h	+25 deg	PanSTARRS Photometric Reference Ladder, SDSS

Note: As of February 2016, the ODI PPA team is preparing to use the PanSTARRS catalog as a photometric reference. Once completed, ODI photometry in the g' r' i' z' bands can always be referenced to local standards. u band photometry, however, will remain dependent on being linked to the SDSS catalog.

2. Fringe map: TBD

**Notes:** (neglecting these rules will result in invalid calibration data):

1. A minimum of thirty minutes must pass between powering on the detectors (turning on only the Agilent power supplies does not suffice) and acquiring calibration products. This allows the temperature of the detectors to stabilize; calibration products will be invalid otherwise.
2. Before each set of bias or dark exposures, a CCD Clean needs to be executed.
3. After each saturated test flat field, a CCD Clean needs to be executed





# Appendix A

## Software Operations & Known Issues

### A.1 Known Issues

#### A.1.1 Stargrasp Controllers GH become unresponsive

This problem is under evaluation, and no fact-based mitigation strategy is known. The best at the moment is to:

1. Power down all detectors. The Exposure GUI will lock up - restart it.
2. Power cycle the GH power supplies at the power supply box.
3. Go through the entire startup sequence (Warmstart -> pon -> ... )
4. If not successful, the exposure GUI will lock up. Restart it. Rotate the instrument by 90 to 180 degrees. See what happens. If there is a recovery, take it! If not, no idea at this time. Call somebody.

#### A.1.2 Readout stalls for a while, but resumes

There is an unknown lock /race conditions during the image data transfer from the controller to the data acquisition computer. The run.out log on odiweb will contain error messages like "IJCATP error". This error happens after the image is read out of the CCD, i.e., the image itself will not be affected.

This error mode is new, and might have to do with network collisions when a much larger amount of data than for pODI is read out.



Frequency: A few times per night.

Recovery: Once the image has read out (can be delayed by a minute or so), the system should be working nominally.

### **A.1.3 Readout stalls and does not finish, with error messages such as DAC busy.**

This is an internal error in the Stargrasp controllers, from which recovery is not always possible without restarting the controllers.

Frequency: Once every few nights.

Recovery:

- If the Exposure GUI is locked, restart the GUI.
- Initiate a bias exposure. If successful - good! Otherwise:
- Power down detectors. This might stall and block the Exposure Gui; restart GUI in this case. Warmstart controllers, follow the usual startup sequence. Take a test bias to verify that everything works again.

## **A.2 Walkthrough: Bringing up the ODI Observing Environment**

This is the procedure to start from a fresh login to `wiyn-5`.

1. Log in as `odiobserver` at `wiyn-5` in the WIYN control room.
2. Open the ODI Menu.
3. Start the Low-Level instrument controls:  
From the ODI Menu, Start the ISP Menu.
  - (a) From the ISP Tools Menu, start the Filter Interface.
  - (b) From the ISP Tools Menu, start the ADC Interface.
  - (c) Optional: From the ISP Tools Menu, start the Shutter Interface.
4. Launch the data inspection & guide star tools:
  - (a) From the ODI Menu, launch the ODI File Browser
  - (b) From the ODI Menu, launch the OTAListener





- (c) From the ODI Menu, launch the Telescope Guider
5. Launch the IRAF system:
- (a) From the ODI Menu, launch *vocl*.
  - (b) From the ODI Menu, launch *DS9*.

## A.3 Starting and Shutting Down the ODI Computer System

### A.3.1 Restarting the JBOSS Application Server on odiweb

At the core of the ODI data acquisition system is a JBOSS application server; this JBOSS server is hosted on the machine `odiweb.kpno.tuc.noao.edu`. By default, the JBOSS server will automatically start when `odiweb` is booted.

Under some circumstances it might be indicated to restart the application server; this is the case for new software releases (in which case a restart is initiated by WIYN personnel), or when the data acquisition system enters an erroneous state.



#### Notes:

1. Under normal circumstances, there will always be an instance of JBOSS running on `odiweb`, even if no ODI interfaces run on the observer machine (`wiyn-5`). Never start a second instance of JBOSS!
2. The JBOSS instance is also responsible for health monitoring ODI. *Never* shut down JBOSS without immediately restarting a new instance! Without `odiweb` or JBOSS on `odiweb` running, health monitoring does not operate.

To start the JBOSS application system:

1. Login to `odiweb`:  

```
ssh odiobserver@odiweb.kpno.noao.edu
cd ODIRun
```
2. Ensure that no instance of JBOSS is running on `odiweb`:  

```
ps aux | grep jboss
```

If an instance is running, first gracefully shut it down (see below), or when grace is not appreciated, use `kill`.
3. Start JBOSS:  

```
nohup ~/jboss-5.1.0.GA/bin/run.sh -b 0.0.0.0 >run.out 2>& 1 &
tail -f run.out
```

To gracefully shut down JBOSS:

1. Login to `odiweb` (see above)
2. `~/jboss-5.1.0.GA/bin/shutdown.sh -S`



### A.3.2 Restarting the JBOSS Application Server on odiserv

The JBOSS system on `odiserv` manages aggregation of metadata from the telescope control system and the transport of images to the PPA system.

To start/stop the JBOSS system on `odiserv`:

- `ssh root@odiserv`  
`cd ODIRun`
- To start if no JBOSS is running:  
`nohup /jboss-5.1.0.GA/bin/run.sh -b 0.0.0.0 > run.out 2>&1 & tail -f run.out`
- To halt JBOSS:  
`/jboss-5.1.0.GA/bin/shutdown.sh -S`

### A.3.3 Starting the ODI Database System (Oracle)

An ORACLE database running on `odiserv` is storing instrument telemetry and is a crucial backbone for FITS header population. To start /stop the ORACLE database:

- `ssh root@odiserv`  
`su oracle`
- To start ORACLE:  
`cd ~`  
`./oraclestart`
- To stop ORACLE:  
`cd ~`  
`./oraclestop`



## Appendix B

# Starting Observations on the Command Line

While observations can be manually invoked on the command line, this is not the recommended mode for a regular observer. Using the command line will not properly fill metadata about data ownership and is thus incompatible with the ODI PPA system. The only acceptable use of the command line tool is during:

1. Engineering observations
2. Commissioning of ODI
3. Non-standard observations

To start the manual observer mode, open a shell window and ssh as `odiobserver` to the computer `odiweb`; there, go to the sub-directory `prod`:

```
ssh odiobserver@odiweb
cd prod
```

Additional setup might be required to define the current program and principal investigator. Commands will be invoked using `ant`:

- `ant coldstart`  
Power-cycle on Stargrasp power supplies and boot stargrasp controllers
- `ant powerdown`  
Power off the Stargrasp Controllers. The Agilent power supplies remain on.



- ant warmstart  
Boot the Stargrasp Controllers
- ant pon  
Power on the OTA detectors
- ant pof  
Power off the OTA detectors
- ant cleanStargrasp  
Clean detectors
- ant calibrate\_dr  
Calibrate the pedestal level of the Stargrasp controllers
- ant bias -D\_COMMENTS="Comment"<sup>1</sup>  
Acquire a bias frame.
- ant bias\_dr -D\_COMMENTS="Comment"  
Acquire five bias frames in a row.
- ant dark\_dr -D\_EXPTIME=[exptime] -D\_COMMENTS="Comment"  
Acquire a dark with the given darktime
- ant dflat -D\_EXPTIME=[exptime] -D\_COMMENTS="Comment"  
Acquire a dome flat with the given exposure time
- ant exposeIndex\_dr -D\_EXPTIME=[exptime] -D\_COMMENTS="Comment"  
Acquire a static exposure without telescope guiding
- ant preimage -D\_PREEXPTIME=[exp time [s] for preimage] -D\_VIDEXPTIME=[exp time [s] for video] -D\_EXPTIME=[static exposure time] -D\_COMMENTS="comments"  
Acquire a static exposure w/ telescope guiding. Guide star will be manually selected form guide star using OTAListener.

Data products are currently stored to (as seen on wiyn-5):  
/Volumes/odifile/archive/pODI/TEST-12B-2101/[Date]

---

<sup>1</sup>Do not include „=“, „/“ in the comments!

## Appendix C

# When Images Look Wrong

When the detector array is not properly configured, or the instrument is in a wrong state, images can look very different from their normal behavior. We discuss such situations below.

### C.1 Flat Field: The Tertiary Mirror at Wrong Port

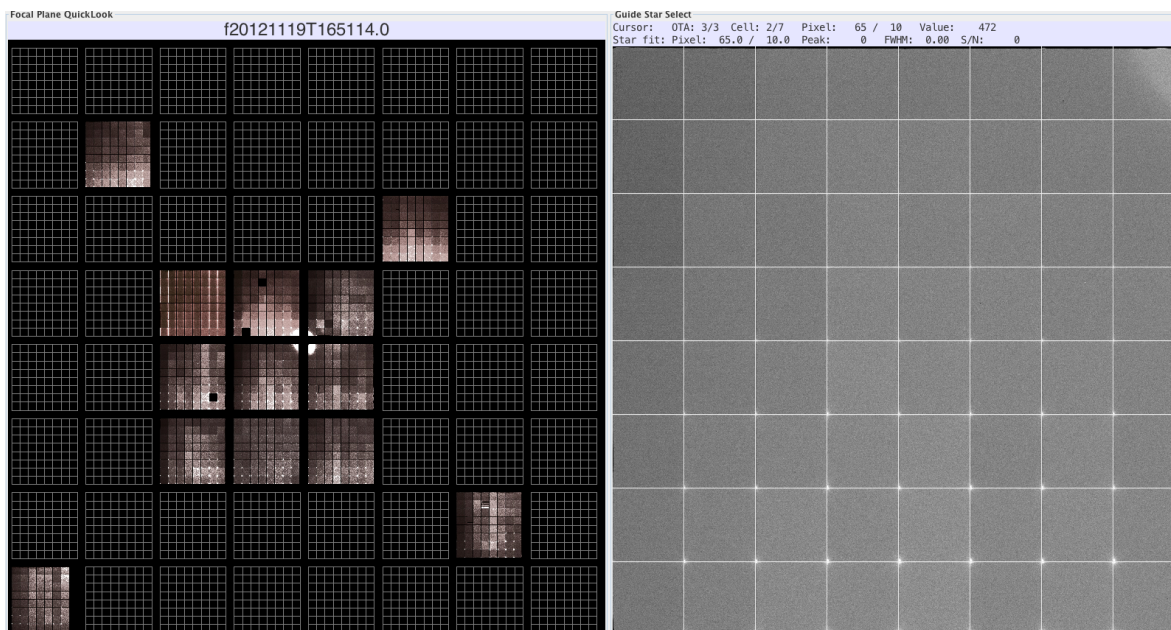


**Figure C.1:** A flat field when the tertiary mirror points to the wrong port. Little light will be received by the focal plane.

## C.2 Condensation on Dewar Window

Despite purging the dewar window with dry air, it is vulnerable to condensation under high humidity conditions (when humidity is higher than 80%). Condensation will typically start at the center of the window where the dry air flow is lowest. Symptoms include haze around bright stars and disappearing stars towards the center of the field of view (see Fig. C.2). A typical indication of onsetting window fogging is that for short exposures there is no problem, but when the shutter is opened for a prolonged time, the dewar window is consequently exposed to more moist air. Closing the shutter will allow the dry air to fight the condensation again.

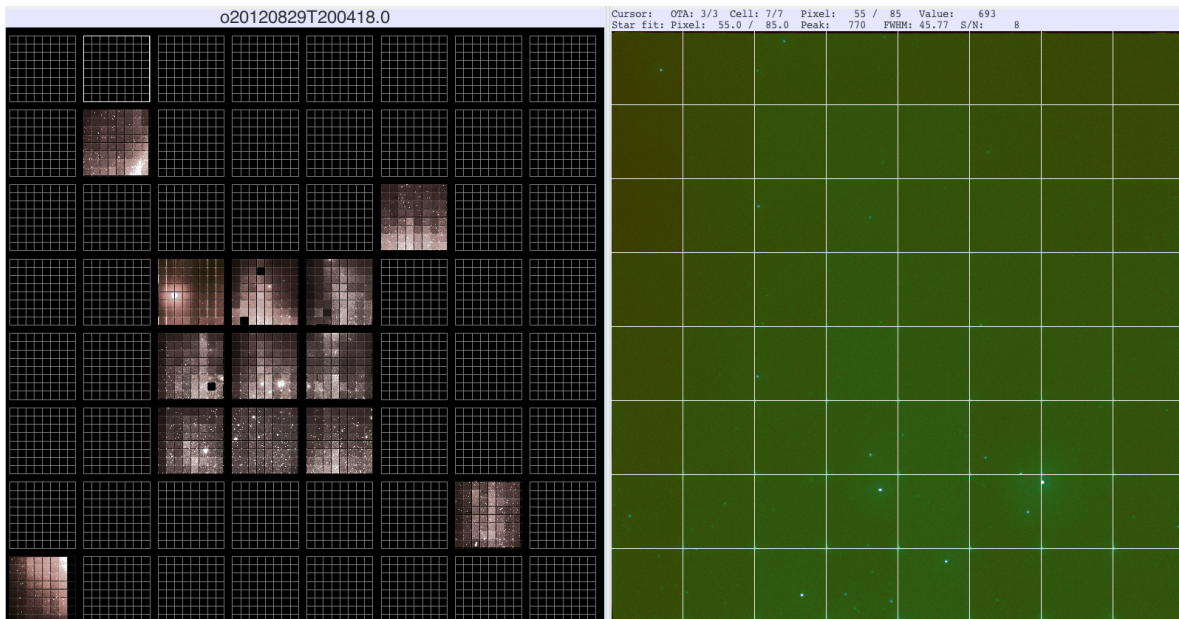
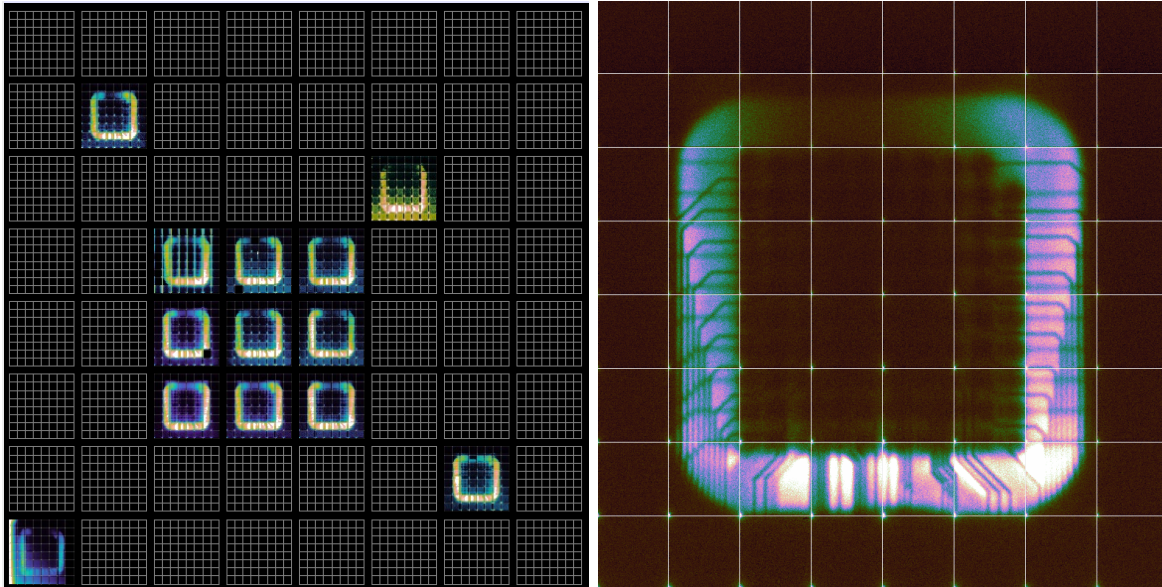


Figure C.2: Example of condensation on the dewar window.

## C.3 Vacuum Ion Gauge enabled

The vacuum gauge in the ODI dewar has a fine-vacuum mode using an ion gauge sensor. Ions are created by a heated, and hence glowing wire, bringing light to the darkness of the dewar. When in the ion-gauge mode, the glowing filament is an efficient back-illuminator of the focal plane, and interesting structures of the OTA detectors become visible „X-ray” style. The obvious structures are: (i) the detector’s ceramic package, (ii) wire traces in the package, and (iii) the 10 pin-grid array. If your bias looks similar to Fig. C.3, ask the telescope operator to turn off the ion gauge and repeat your observations.





**Figure C.3:** Bias image taken with the ion vacuum gauge switched on.

## C.4 Residual Charge in Detectors I: After Powering On

## C.5 Residual Charge in Detectors II: Darks

While the gross amount of residual charge seems to clear out fast, there can be a resilient amount of low level charge left in an OTA detector even after power cycling it. This amount will be apparent only in longer dark frames, but can have a dramatic effect with an elevated background level of about 100 ADU. Fig C.5 shows an example of pronounced structure in a dark that was taken without properly cleaning the detectors after powering them on. To correct this problem, follow the detector charge cleaning procedures.

The visible structures have the imprint of the detector package and structure of the wafers on which the detectors were built.

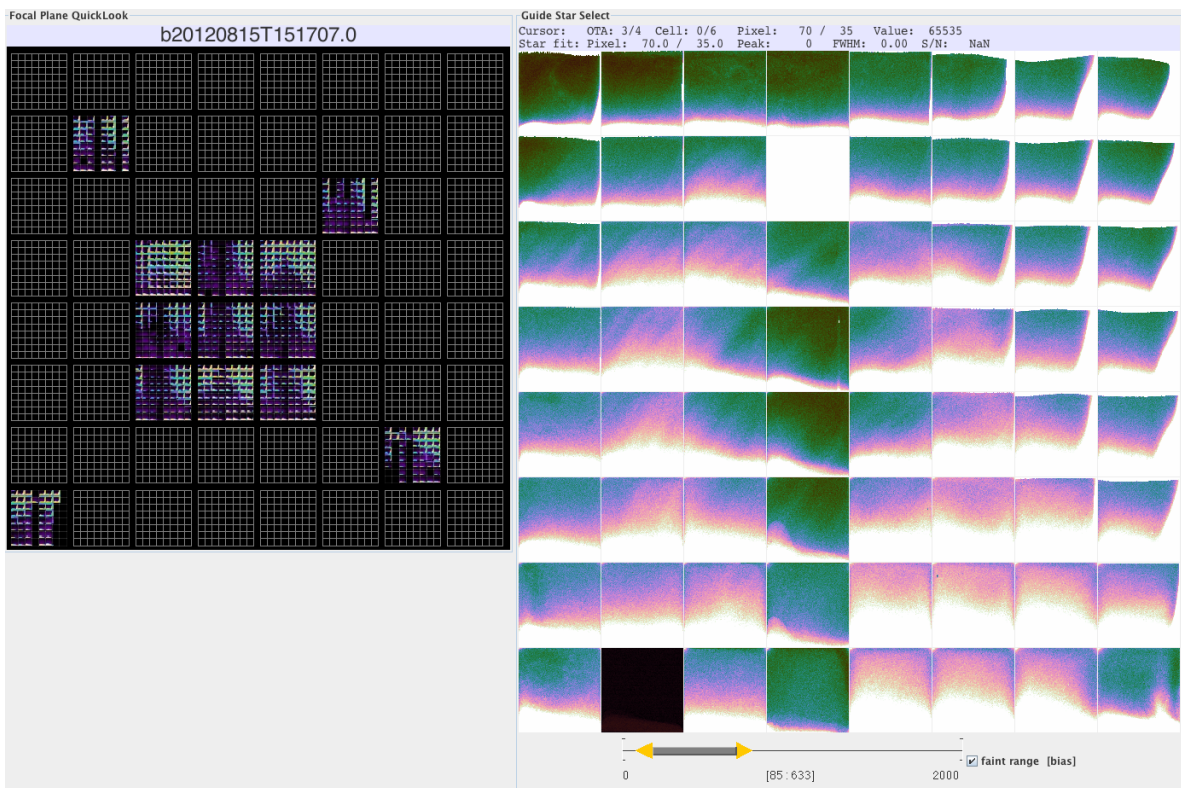


**Figure C.4:** After powering on the OTA detectors, they will probably have residual charge in their imaging area. Reading a few bias images will clear out the detectors.

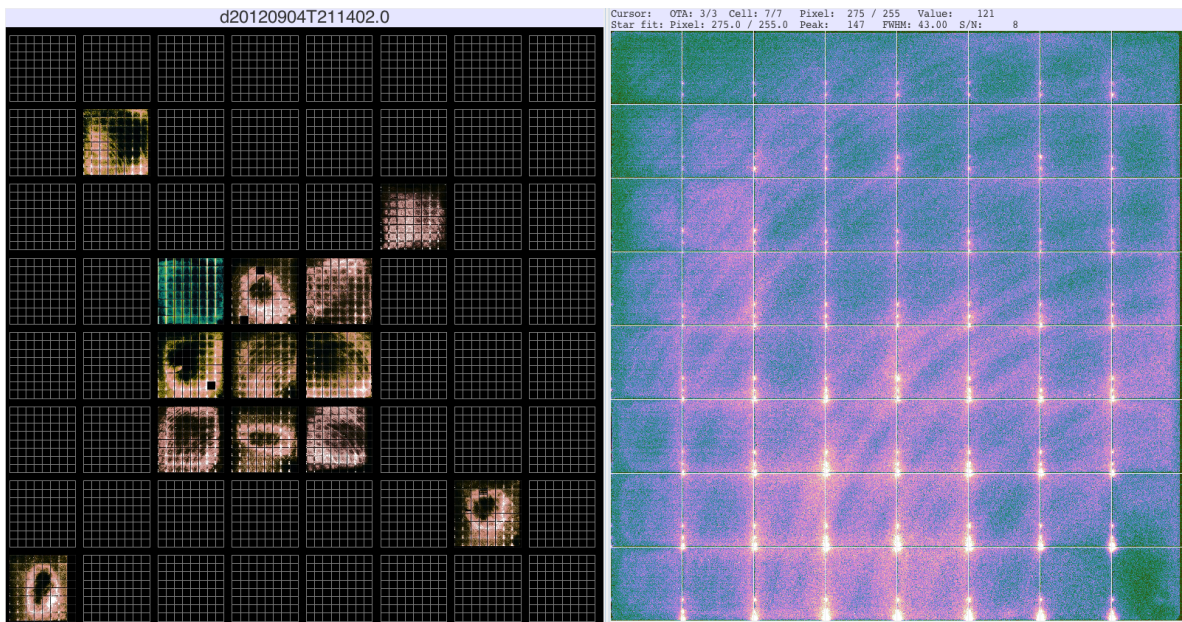


**Figure C.5:** 300 second dark taken after powering on the focal plane array, but without proper charge cleaning.



# Bibliography

Magnier, E. A., Schlafly, E., Finkbeiner, D., et al. 2013, *ApJS*, 205, 20

Rajagopal, J., Harbeck, D., Corson, C., et al. 2014, *SPIE Conference Proceedings*, 9152-70

Tonry, J. L., Stubbs, C. W., Lykke, K. R., et al. 2012, *ApJ*, 750, 99





